UiT
THE ARCTIC UNIVERSITY OF NORWAY

Faculty of Science and Technology

Department of Physics and Technology

Wind Energy at Nygårdsfjellet - Norway

Wind field characterization and modelling

—

Muhammad Bilal

A dissertation for the degree of Philosophiae Doctor – September 2016

UNIVERSITY OF TROMSØ

Dedicated to my mother, Tasneem Hafeez.

Abstract

The research focuses on the characterization of wind flow over complex terrain of Nygårdsfjell and numerical wind flow modelling. In the context to research focus, the main contributions of this research thesis are within the following areas:

Characterization of wind flow at the Nygårdsfjell wind farm, situated above the Arctic circle in Norway. Wind data is collected from the anemometers installed on the wind turbines and thereafter analysed for understanding the existing wind patterns. The analysis established existence of bi-directional high winds at Nygårdsfjell wind farm particularly during colder periods.

Computational fluid dynamic (CFD) solver FLUENT is used to model the wind fields over the complex terrain of Nygårdsfjell. Overall, the shear stress transport model gives good simulation results that explains the speed up effects at the turbine location, which makes the wind farm a suitable site for wind energy.

Local terrain effects on the wind flow over Nygårdsfjell are modelled by coupling meso-micro scale models. One set of meso-scale winds are generated from Weather Research and Forecasting model, whereas the other set is taken from the Modern-Era Retrospective Analysis for Research and Applications dataset. CFD based numerical solver, WindSim, is used as micro-scale coupling partner. One of the proposed coupled models achieved improvements in wind speed modelling.

A basic method for preliminary wind resource assessment at remote sites is proposed. The method is a combination of interpolation and extrapolation of wind data from the surrounding sites to the potential wind farm site. However, due to large disparities between the terrains and conditions, the results from this project does not contribute directly to the main research area.

Acknowledgments

All praise is due to ***Allah***.

First, I would like to thank my supervisors Yngve Birkelund and Guillermo Araya. I am grateful for your supervision and input in my thesis. Yngve, I am especially grateful for your quick reading and useful comments in these last weeks before submission. Special thanks to Rune for always helping me understanding various meteorological phenomena.

During my PhD, I had the pleasure of staying six months at the Texas Tech University, Lubbock, USA. I would like to thank Guillermo Araya, KV Praju, Archie Ruiz, Narendran Sridhar and the rest of the group members for their hospitality, thoughtful support and stimulating discussions. Specially, I would like to thank Praju for helping me learning WRF model.

I am sincerely grateful to Nordkraft AS and especially Matthew Homola for providing me all-important technical support and field measurement data as well as conducting LIDAR measurement campaign with me. I would also like to thank Muhammad Shakeel Virk for his insights and guidance on a research project.

I am very grateful to all the co-authors of my research papers.

I enjoyed my stay at UiT very much and made many valuable friends. Big thanks to Adnan, Balpreet, Bilal, Cheema, Cristina, Elia, Emma, Firehun, Gema, Jakob, Jonas, Kine, Kjell, Maria, Pascal, Rajan, Ralph, Sakis, Sanat, Sean, Silje, Stine, Temesgen, Terjei, Thomas B, Thomas K, Wasif, and Yasin, all have been a big help to me during my thesis as well as having a very enjoyable time.

Special thanks to Stallo technical support - especially Jan and Espen - without their support it would not have been possible to run WRF simulations for one year during such a short time.

Many thanks and appreciations to Torgeir, who have been a massive help in sharing matlab codes and extending full help.

I am deeply indebted to my mom; you are the greatest person in my life. I sincerely appreciate all the sacrifices you made for us. I am lucky to have such a sister who always extends her unconditional support to me.

Finally, I would like to thank my amazing wife, Gulcin Yazici, for bearing with me during this time-consuming process. I am very thankful for her unbounded patience, love and care.

Contents

Chapter 1

Introduction

1.1 Research development and outline

Nygårdsfjell wind farm, located above the Arctic circle, has been reported to experience favourable wind conditions for harnessing wind energy. The location of the wind farm makes it an obvious choice to conduct wind research in North Norway. The research focuses on the characterization of wind flow over complex terrain of Nygårdsfjell and numerical wind flow modelling.

Cold climate regions have unique environment conditions, which are considerably different from other parts of the world. International Energy Agency - Task XIX Wind Energy R&D is formed to develop effective technologies by learning from the shared experiences of operating wind farms in such conditions around the world. The cold climate regions have a large wind power potential (Krogsgaard et al., 2013; Tammelin et al., 1997; Baring-Gould et al., 2010; Wind, 2011; Leclerc and Masson, 2003; Laakso et al., 2003; Lacroix and Manwell, 2000; Homola, 2005). North Norway is one of the few places in the world where cold climate unites with complex terrain. That emphasizes the importance of understanding the challenges presented by not only cold climate but complex terrain as well. Krüger et al. (2014) evaluated the wind flow over the complex terrain of lake Wannsee in Berlin, Germany. The simulations are carried out by means of the shear stress transport turbu-

lence closure in a Reynolds averaged Navier-Stokes approach and it is found that the local terrain has a significant impact on the flow field. CFD based wind prediction methodology using measurements from real wind farms over complex terrain provided improved agreement with measurements when compared to the linear flow models (Manning et al., 2011). Gravdahl et al. (2002) showed that power production from different wind turbines varies up to 25 % even though the variation in ground elevation was only 7 meters. Further, a redesign of the wind farm layout based on simulations would give a 10 % increase in the energy production. Beside CFD methods, meteorology based models have also proven themselves very useful in predicting various environmental variables, partly because they are equipped with the possibility of wide range of configurations (Byrkjedal and Berge, 2008). This diversity also poses a challenge to find the right set of configurations and the numerical and physical schemes that are also dependent on the multidimensional and nonlinear interactions (Nossent et al., 2011). The first and the foremost challenge is to find the correct combination of configurations of the model to use in a specific area. The best configuration for one area might well not be suitable to other areas (Krieger et al., 2009).

In the context to previously reported work, the current research is an attempt to understand wind flow under cold climate of Nygårdsfjell and model it over its complex terrain. One year site data is analysed to characterize the wind circulation over the complex terrain of the Nygårdsfjell wind farm. The main pattern found, is that the wind is either coming from east or from west. A clear bidirectional wind pattern, following the local terrain around the wind farm. Two nearby places seemed to be contributing to the wind pattern over the wind farm beside the complex terrain of the larger region. The Ofotfjord in west and the Torneträsk lake that is situated some 60 km in east. Torneträsk usually remains under ice during winters and most of the spring season whereas Ofotfjord remains relatively at warmer temperatures throughout the year. Torneträsk lake is a top suspect as source of cold winds that pass over Nygårdsfjell wind farm before they fade into Ofotfjord. The lake is surrounded by high mountains and it works as a basin for the cold winds that slide from the surface of ice covered mountains. The air then spills towards the west while the local terrain channel and boost these winds until they disappear into Ofotfjord. This hypothesis is tested by analysing the one-year observational data (May 2008- April 2009) at the Nygårdsfjell wind farm. The results and choice of data analysis are presented in attached

manuscript **Paper I**. Summarising the results; it is found that around 85 % of the high wind events occurred during the colder periods. A high wind event is defined as the period of time when wind speed is equal or higher than 12 m/s. The overwhelming majority of these high winds are coming from east of the wind farm. The analysis also established the existence of bi-directional - eastern and western wind flows at Nygårdsfjell wind farm with almost negligible winds coming from elsewhere.

Computational fluid dynamic (CFD) technique is used to investigate the possibility of modelling wind flow over the complex terrain of Nygårdsfjell. CFD ANSYS Fluid is used with three models to simulate the wind flow. Experimental setup and finding of the project are documented in attached manuscript **Paper II**. To summarise the results, it is evident that the wind farm terrain indeed has a speed up effect at the location of the wind turbines, making the wind farm an ideal location for extracting wind energy. The simulations also showed the negative wind shear that may translate to higher mechanical loads on the wind turbines.

CFD based micro-scale modelling tool, WindSim is coupled with meso-scale wind generated from the Weather Research and Forecasting model (WRF). WRF is a numerical weather prediction tool. WRF is run to model three selected cases from findings of Paper I. The three cases are selected from different seasons in an attempt to capture the seasonal variations. The main objective is to evaluate whether using the meso-scale winds as input to WindSim can improve the performance of micro-scale model. WindSim tend not to solve the motion equations and work solely according to the initial and boundary conditions. Feeding WindSim with values that have been solved using the motions equations, as in case of WRF, might improve the results. For comparative study, another set of meso-scale winds were taken from the Modern-Era Retrospective Analysis for Research and Applications (MERRA) data system. The experimental setup and corresponding results are compiled as attached **Paper III**. To summarise the findings, the meso-microscale based WRF-WindSim coupling model showed a better solution for predicting the wind flow over the complex terrain of Nygårdsfjell than the MERRA-WindSim coupling for the given data set.

Further, a basic wind resource assessment technique is evaluated at a remote site by using the closest available neighbouring sites having field measurements. The main motivation originated from the fact that field measurement data is very scarce at suspected good sites for wind energy in north Norway. The campaign to gather authentic field data can last several years besides being very resource demanding in such challenging conditions. The basic idea is to use the neighbouring available wind resource data (metrological or other) to conduct a preliminary wind resource assessment at a site of interest. The proposed technique extrapolate the neighbouring winds to heights where the terrain effects become negligible. The case here is to identify the wind resources in general at the site of interest irrespective of the direction they originate from and the local speed up effects. After extrapolation, a plane is interpolated over the site of interest. The wind can then be reverse extrapolated to turbine location at the site of interest. This technique is tested at a single site on limited dataset in West Texas USA. The findings of the project are compiled in attached **Paper IV**. The conditions and situation at West Texas strongly disagree with the complex terrain at Nygårdsfjell wind park. Thus, we cannot apply these results directly into our main research question.

1.2 Site description

The Nygårdsfjell wind farm, a complex terrain above the Arctic circle and near Norwegian-Swedish border, is the main site for the research. The Nygårdsfjell wind farm is located in a valley at approximately 420 meters above sea level with mountains up to 2000 meters in north and south. A mountainous terrain with lower gradient goes east towards Torneträsk, a 330 square km lake that also acts as a natural wind channel, and is surrounded by higher mountains predominantly in north and south. Ofotfjord is located 9 km south-west of Nygårdsfjell wind farm. Ofotfjord is ice-free and relatively warm during the winter due to the Gulf Stream. Figure 1.1 shows the general terrain of the area with white box highlighting the location of the wind farm.

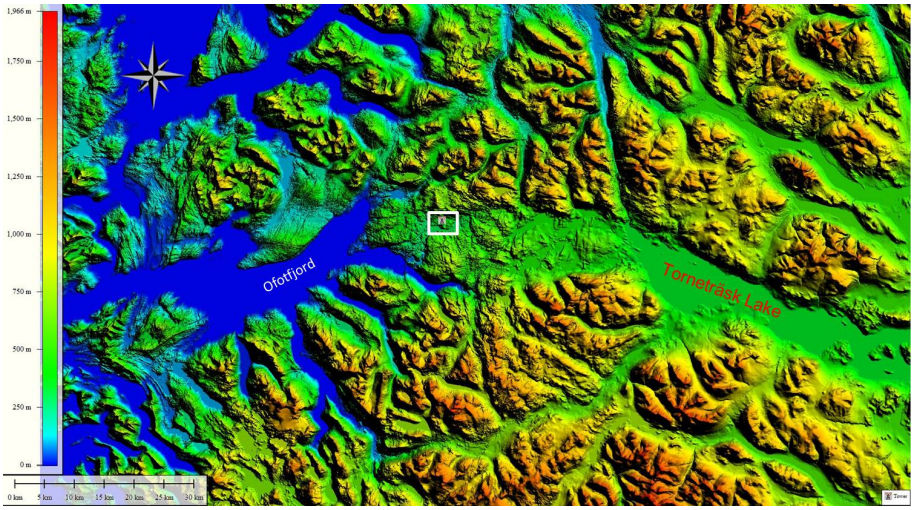

Figure 1.1: General terrain of the area along with Nygårdsfjell wind farm

1.3 Thesis structure

Chapter 2 describes wind speed and its most relevant characteristics. Last section of the chapter discusses the measurement data at the Nygårdsfjell wind farm. Chapter 3 describes WRF and discusses simulation setup and modelling results at the wind farm. Published research papers are attached in Chapter 4. Finally, the conclusion and future research possibilities are given in Chapter 5.

1.4 Description of publications

Paper I

Muhammad Bilal, Yngve Birkelund, and Matthew Homola, "High winds at Nygårdsfjell", Journal of Clean Energy Technologies, vol. 3, no. 2, p. 106-109, March, 2015.

My contribution is data analysis and writing the first draft. Matthew Homola provided the measured data and commented on the draft. Yngve Birkelund helped to improve the paper by providing comments.

In Paper I, we investigated the presence of high winds at the Nygårdsfjell wind farm, situated above the Arctic circle in Norway. Wind speed data was collected from the anemometers installed on the wind turbines and thereafter analysed. The measurement equipment was well maintained during observation period. The selected observation period presents a typical year at the wind farm. The findings of the paper supported the initial hypothesis of dominant winds being generated from east of the wind farm and spills westward towards the Ofotfjord creating high wind events at the Nygårdsfjell wind farm. The results of the paper are very clear that rules out any doubts about the shortcoming of the sensors on the nacelle to capture the free stream wind. Any uncertainty in this regard, if at all, would be of minor importance.

Paper II

Muhammad Bilal, Guillermo Araya, Yngve Birkelund, Narendran Sridhar, and Siva Parameswaran, "Wind Flow Over a Complex Terrain in Nygårdsfjell, Norway", ASME, Paper No. ES2015-49188, pp. V002T19A005; 9 pages, July, 2015.

My contribution is main idea, input data and writing the first draft. Narendran Sridhar did the simulations and analysis. Guillermo Araya helped with analysis and conclusion. Yngve Birkelund and Siva Parameswaran commented on the manuscript.

In Paper II, we attempted to model the wind flow over complex terrain of Nygårdsfjell by using computational fluid dynamic (CFD) techniques. Three CFD models were used and the shear stress transport model gave good simulation results. The study highlights the natural tunnelling effect of the terrain and speed up effect at the Nygårdsfjell wind farm. That explains the favourable wind conditions for the wind turbines. On other hand the negative wind shear indicated by the model describes the potential high loads on the turbines.

Paper III

Muhammad Bilal, Yngve Birkelund, Matthew Homola, and Muhammad Shakeel Virk, "Wind over complex terrain - microscale modelling with two types of mesoscale winds at Nygårdsfjell", Renewable Energy Journal, vol. 99, p. 647-653, July, 2016.

My contribution is conducting the simulations, doing data analysis and writing the first draft. Matthew Homola and Yngve Birkelund revised the manuscript. Muhammad Shakeel Virk commented on the paper.

In Paper III, we evaluated the feasibility of using meso-scale winds as input to micro-scale model. Two sets of meso-scale winds are used for this research work. The WRF data is generated by setting up simulations centred around the Nygårdsfjell wind farm whereas second set of meso-scale winds are taken from the Modern-Era Retrospective Analysis for Research and Applications (MERRA) data system. WRF is setup using the PBL scheme; local closure turbulent kinetic energy scheme Mellor-Yamada-Janjić along with the short/long wave radiation scheme Goddard. The selected PBL setting may not be optimal for this site, but are similar to previous settings that have been used with success in other research work. WindSim, a computational fluid dynamics based numerical solver, is used as micro-scale modelling tool. We have followed the user manual of the WindSim for setting up the model and running the simulations. It is important to mention here that, this is not the preferred method of meso-microscale model coupling, but this method is evaluated as it was expected to be easier to implement and to check if it could still give valuable results. The proposed method is applied to three selected cases due to resource constraints. The intention of the work is to introduce a potentially promising method that is recommended to be tested

on larger data sets. The meso-microscale based WRF-WindSim coupling model showed a better solution for predicting the wind behaviour over the complex terrain of Nygårdsfjell than the MERRA-WindSim coupling for the given data set.

Paper IV

Muhammad Bilal, Guillermo Araya, and Yngve Birkelund, "Preliminary Assessment of Remote Wind Sites", Energy Procedia, vol. 75, p. 658-663, August, 2015.

My contribution is conducting the simulations, doing data analysis and writing the first draft. Guillermo Araya provided the measured data and revised the manuscript. Yngve Birkelund commented on the manuscript.

In Paper IV, we tested a preliminary wind resource assessment technique that make use of the surrounding measurements. The technique is a combination of interpolation and extrapolation of wind data from surrounding sites to the potential site. The heights selected as basis for extrapolation are the ones with the least error rate. The wind speed is extrapolated to 1000 meters in order to diminish the local terrain effect. A plane is interpolated over the potential site using the neighbouring wind speed values. Results were promising for a limited available data set on a particular site in West Texas, USA. It is important to mention that the investigation was of very elementary nature and lack the data validation over larger data sets and on more complex terrain sites. The calculations are carried out assuming stable atmospheric conditions. The interpolation techniques are used from QGIS software without altering the default parameters. The main objective of the research was to test a potentially user-friendly technique that might have broader applications on various types of sites in future. Unfortunately, we could not acquire more data from other sources to test the technique over complex terrain of north Norway. The intentions were to further test and improve the technique in north Norway.

Chapter 2

Wind

Sun is the main source of energy on the surface of the earth. The unequal heating of the surface of the earth drives wind. Total irradiation of the sun declines from equator to the poles. As a result, there is excess energy in the equatorial zones and less in the polar zones of the atmosphere. For equilibrium, heat is transported by the airflow from equator to the northern and southern polar regions. This is achieved by the air mass exchange of the global wind systems. The global wind system flow is deflected by the presence of Coriolis force due to the rotation of the earth. The surface friction and the atmospheric stability of the atmospheric boundary layer has no influence on the geostrophic or free atmosphere winds. These winds exist high in altitude where pressure gradient force and the Coriolis force are in balance (Emeis, 2012).

2.1 Wind in boundary layer

The atmospheric boundary layer is located below the undisturbed geostropic winds, where the wind speed is strongly varying with the height above the ground. Factors such as friction at the ground, the orography and the vertical distribution of temperature and pressure influence variation of wind speed in this layer. The atmospheric boundary layer can be divided into three vertical

layers. The lowest layer is laminar in nature with only few millimeters in depth and has no direct use for wind energy application. Above it comes the surface layer also called Prandtl layer with a layer thickness up to 100 meters. Within this layer, the turbulent forces dominate and the wind speed has the largest shear. The third layer within the atmospheric boundary layer is called the Ekman layer. In this layer, Coriolis force influences the wind direction with height. The depth of atmospheric boundary layer varies through the day. During night time with gentle winds, it may decrease to about 100 meters, while the strong solar irradiance during the daytime can deepen it to about $2 - 3$ km (Emeis, 2012). Figure 2.1 shows the wind variations in atmospheric boundary layer.

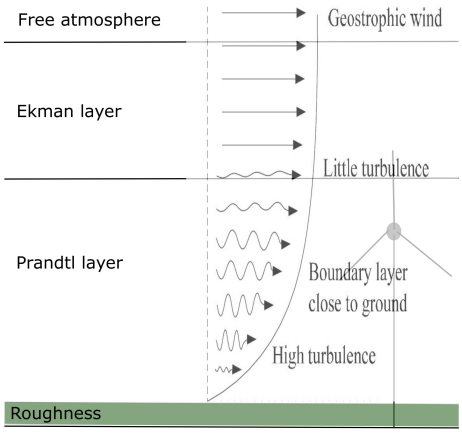

Figure 2.1: Simplified atmospheric boundary layer scheme

Wind turbines operate more or less in the Prandtl layer of the atmosphere. The Prandtl layer is defined meteorologically as that layer where the turbulent vertical fluxes of momentum, heat, and moisture deviates less than 10 % from their surface values and where the influence of the Coriolis force is negligible. Usually this layer covers only 10 % of the whole atmospheric boundary layer depth (Emeis, 2012). In reality, the height of Prandtl layer varies according to the surface friction, wind speed and vertical temperature profile. The extractable energy and loads on wind turbines depend upon the properties and intensity of the air mass within this layer (Gasch and Twele, 2011).

2.2 Vertical wind profile

Wind variations with height, also known as wind shear or height profile or vertical wind profile, is the most important atmospheric feature for the energy extraction from the wind. Furthermore, the variable wind exerts different loads on the wind turbine structure including the rotor. The terrain, surface roughness, topography, vertical temperature profile and the atmospheric conditions influence the vertical wind profile.

2.2.1 Atmospheric stability

Before discussing the atmospheric stability, some basic terms are needed to be defined. An **air mass** is a well defined body of air with constant number of molecules that act as a whole. It does not readily mix with surrounding air and the heat exchange between the air mass and surrounding air is minimal. The temperature within the air mass is generally uniform. Atmospheric pressure and temperature influence the vertical motion of air mass. Keeping other factors constant, temperature of the air mass increases with increasing pressure and vice versa. The **lapse rate** is defined as the rate at which air temperature changes with height. The environmental lapse rate is a result of complex meteorological factors and usually taken as decrease in temperature with height. Air mass with higher temperature than surrounding environment will expand and begin to cool down. As long as the air mass is at a higher temperature than surrounding environment, the air mass is less dense and will keep rising. But as the air mass expands its pressure is decreased and therefore its temperature decreases as well. At a point where the temperature of the air mass equals the temperature of surrounding environment, the air mass neither rises nor sinks unless influenced by external factors such as wind flow. When the temperature of the air mass is less than the surrounding environment, the air mass gets dense and sinks. The extent of atmospheric stability is determined by the vertical temperature profile (Barry and Chorley, 2009; Curry and Webster, 1998). The three states of atmospheric stability are discussed in the following sections.

2.2.1.1 Unstable

Under unstable atmospheric conditions, the air mass closer to the ground gets warmer than the surrounding environment. It may be because it is heated by the earth's surface. This typically happens in summer when the sun heats up the land rapidly. In this situation the surrounding environment has a lapse rate greater than the lapse rate of air mass, so that the rising air mass will continue to be at warmer temperature than the surrounding environment. In this situation, considerable vertical mixing is expected upwards and downwards. The degree of instability is dependent upon the magnitude of difference between the lapse rates of air mass and the surrounding environment. The strong vertical mixing under unstable conditions causes turbulence and a small gradient of the wind speed with altitude (Gasch and Twele, 2011). Figure 2.2 shows the influence of unstable atmospheric conditions on vertical wind profile.

2.2.1.2 Neutral

If the atmospheric stability is neutral, then surface boundary layer neither heats up nor cools down. In this situation, the air mass lapse rate is the same as the surrounding environmental lapse rate. Vertical displacement of air mass is neither encouraged nor discouraged. The vertical wind profile does not depend upon the thermal stratification of atmosphere rather only on surface friction (Gasch and Twele, 2011). This condition is most likely to occur during high wind speeds and when there is sufficient cloud cover preventing strong heating or cooling of the earth's surface. The continuous line in figure 2.2 shows the vertical wind profile under neutral conditions.

2.2.1.3 Stable

During stable atmospheric conditions, the air mass has higher lapse rate than surrounding environment. The air mass in this case is stable and resists any vertical movement. In case of lifting by an external factor such as wind flow, the air mass remains cooler and denser than the surrounding environment. Once the external influence is removed, the air mass that has been lifted will

come back to its original position. This usually happens at night times with little or no winds. There is a high wind shear under stable conditions (Gasch and Twele, 2011). The vertical wind profile is shown as dotted line in figure 2.2 under stable conditions.

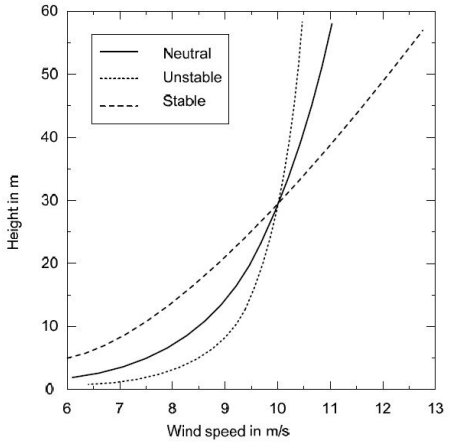

Figure 2.2: Vertical wind profile under different atmospheric conditions (Petersen et al., 1997)

2.3 Vertical interpolation

Under neutral atmospheric condition above absolutely flat surface with uniform roughness length, the increase in wind speed with the height within the prandtl layer is given by Hellmann power law (Lloyd, 2003),

$$\frac{v(z_1)}{v(z_2)} = \left(\frac{z_1}{z_2}\right)^{\alpha}, \tag{2.1}$$

where $v(z_1)$, $v(z_2)$ are the wind speeds at the heights z_1 and z_2 respectively, α is called the power law exponent, also known as empirical wind shear component, and its value for normal conditions is 0.14 (Petersen et al., 1997). In reality it is a difficult task to calculate α since it depends upon the roughness length, atmospheric stratification, nature of terrain and orography. By applying reverse mathematics α can be calculated for a specific site. In that

case its application to other sites are not permitted and it is only limited to the individual site.

Logarithmic law is another way of calculating the wind under neutral atmospheric conditions at different heights and it is based upon the boundary layer physics of Prandtl. It considers the roughness length as well and is stated by the equation 2.2 (Gasch and Twele, 2011),

$$v(z) = \frac{u*}{\kappa} \ln\left(\frac{z}{z_0}\right), \tag{2.2}$$

where z is the height, $u*$ shear stress velocity, z_0 roughness length and κ is Kármán constant, which is usually assumed to be 0.4. Application of logarithmic law to two different heights gives a very useful relationship (Gasch and Twele, 2011),

$$v_2(z_2) = v_1(z_1) \cdot \frac{\ln\left(\frac{z_2}{z_0}\right)}{\ln\left(\frac{z_1}{z_0}\right)}, \tag{2.3}$$

where by calculating wind speed v_1 at a height z_1, the formula allows to calculate the wind speed v_2 at a height, usually at hub height, z_2 for the known roughness length z_0. Table 2.1 shows the typical values of z_0 for different types of terrains.

Type of terrain	z_0 **in meters**
Calm water	0.0001 - 0.001
Farm land	0.03
Heather with few bushes and trees	0.1
Forest	0.3 - 1.6
Suburb, flat building	1.5
City centers	2.0

Table 2.1: Roughness length values according to terrains (Gasch and Twele, 2011)

Both of the above mentioned laws are only valid under neutral atmospheric conditions, idealized absolutely flat surface with uniform roughness length.

Variation in temperature profile influences the vertical mixing, the turbulence, the wind profile and eventually the wind speed shear. A correction term is added to the logarithmic wind profile (equation 2.2) to consider the atmospheric stratification due to the changes in temperature profile (Gasch and Twele, 2011),

$$v(z) = \frac{u*}{\kappa}\left(\ln\left(\frac{z}{z_0}\right) - \psi\left(\frac{z}{L}\right)\right), \tag{2.4}$$

where ψ is the empirical stability function that takes into account the influence of the thermal stratification of the atmosphere. It assumes positive value for an unstable, negative for stable and evidently zero for the neutral atmospheric conditions. L is called the Monin-Obukhov stability length. It describes the vertical mass exchange due to the ratio of friction forces and lift forces (Obukhov, 1971). Monin-Obukhov stability length can be estimated from the tables stating its dependence on the z_0 and the atmospheric stability in the German Technical Instructions on Air Quality (Hansmann, 1987).

Both, logarithmic and power law, are valid over absolute flat surface and even terrain. In reality, the terrain of the area may have significant influence over the wind profile. Fluid mechanic techniques are still not sufficient to capture these effects on wind profile. Over a complex terrain, the wind speed is accelerated when flowing over the hills and mountains top. If the slope is very steep, flow separation occurs on the downhill side of the hill. The intensity of the turbulence depends upon the inclination of terrain, temperature profile and on the surface roughness of the area. Figure 2.3 describes the wind flow over complex terrain with steep inclination.

2.4 Horizontal interpolation

The roughness length has a direct influence on the vertical wind profile (Gasch and Twele, 2012). The roughness length itself varies horizontally and depends upon the terrain of the area. For wind energy application, the value of roughness length needs to be calculated over larger areas surrounding the wind farm. Horizontal interpolation of wind speed is also a useful

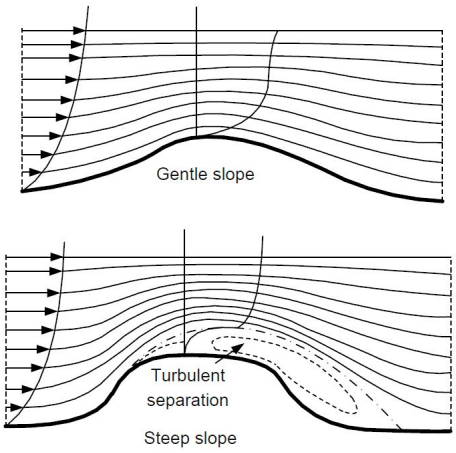

Figure 2.3: Influence of complex terrain on wind profile (Gasch and Twele, 2012)

technique to understand the variations in wind speed over larger areas.

2.4.1 Inverse Distance Weighting

Inverse Distance Weighting (IDW) is one of the deterministic methods of interpolation that combines the idea of vicinity adopted by Thiessen polygons (Thiessen, 1911) with the steady change of a trend surface. Measured values closest to the prediction location will have more influence on the predicted value than those farther away. This distance-decay approach has been applied widely to interpolate climatic data (Legates and Willmott, 1990; Stallings et al., 1992). IDW assumes that each measured point has a local influence that diminishes with distance. The common expression is,

$$Z_{prd}(s_o) \equiv \left[\sum_{i=1}^{N} w(d_i) \cdot Z_{obs}(s_i)\right] / \left[\sum_{n=1}^{N} w(d_i)\right], \tag{2.5}$$

where $Z_{prd}(s_o)$, $Z_{obs}(s_i)$ represent the predicted and observed values at s_o and s_i, N is the number of measured points, *w(d)* is the weighting function, and d_i is the distance from s_o to s_i. The selection of the weighting function has large influence on the output of the interpolation. A number of weighting functions and their merits are analyzed by Lancaster and Salkauskas (1986).

2.4.2 Triangulated Irregular Network

Triangulated Irregular Network (TIN) interpolation is another useful technique. A common TIN algorithm is called delaunay triangulation. It consists of creating a surface formed by the triangles of nearest neighbor points. To do this, circumcircles around selected sample points are created and their intersections are connected to a network of non-overlapping compacted triangles (Tucker et al., 2001; Hutchinson and Gallant, 1999).

2.5 Local winds

The wind systems that are purely pressure driven due to the potential difference in temperature on local or regional scale are called local wind systems. These systems show consistent regularities that make them suitable for the energy generation from the wind. Sea-land breeze and mountain-valley breeze are of most important among the local winds phenomena (Avissar et al., 1990).

2.5.1 Sea-land circulation

A sunny day with a high temperature difference between the land and the water offers the best sea-land wind conditions. This wind condition is diurnal and can be in the order of 100 km. The cause of this wind condition is the fact that during the day the land heats up stronger than the water. The air above it heats up and rise, leaving behind a low-pressure area, which is filled by the cool and humid air coming from the sea. At a higher altitude, the wind flows from land to sea creating a return flow. During evenings, the land cools down faster than the water so the wind flow direction reverses. The wind blows from land to sea but due to the friction of the surface, these winds are much weaker than the winds coming from sea (Gasch and Twele, 2012). Figure 2.4 shows the sea-land circulation.

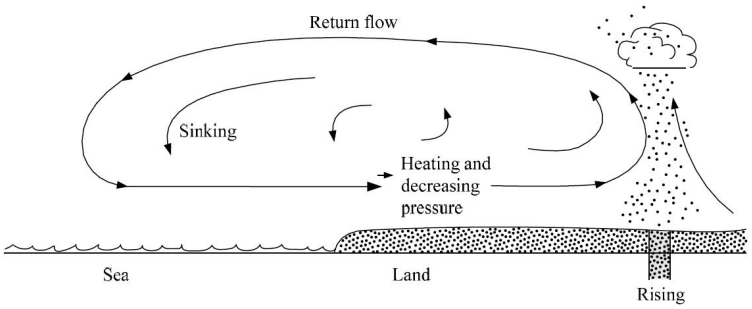

Figure 2.4: Sea-land circulation (Freris, 1981)

2.5.2 Mountain-valley circulations

In the mountains, the wind circulation is often a combination of two flow systems: the slope winds and the mountain-valley winds. During the day, the slopes of the mountains heats up strongly so is the air mass closely above it. The thermal lift of these air mass results into slope winds. The valley winds replace the slope winds from below. At night times it is the other way around. The mountains slopes cools down rapidly causing the air mass closely above it to cool down sharply than the surrounding environment at the same altitude. The gravitational force further drives the denser downhill air mass that accumulates in valley and heads for the exit path. These circulations can be in the order of several tens of kilometers (Vergeiner and Dreiseitl, 1987). Figure 2.5 describe the mountain-valley phenomenon.

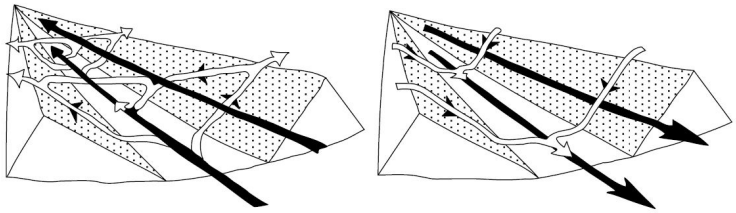

Figure 2.5: Mountain valley circulations (white: slope wind, black: valley wind). Left side: valley winds at day time; Right side: mountain winds at night (Roth, 1989)

2.5.3 Katabatic circulations

Katabatic winds are thermally generated orographic flows that have close similarity with the slope winds. They are based on the principal that colder air is denser and heavier then warmer air. The air mass close to the mountain surface gets colder, denser and slides down the hill with the gravitational pull. Cooling of the land, snow, ice cover and compensating downward sensible heat flux are all a result of long wave radiative energy losses to space. It not only cools the atmospheric surface layer but also forms a temperature inversion. This induces a horizontal temperature gradient over the slopes resulting in a downslope horizontal pressure gradient force, which is the driving force of katabatic winds. These flows are often too shallow to be directly used for the extraction of wind energy. However provided a natural channel within complex terrain and appropriate pressure gradients, these flows can speed up on their way to valley's exit (Anderson et al., 2005; Renfrew and Anderson, 2006).

2.6 Power in the wind

Power from the wind increases as the cube of wind speed so there is considerable incentive to understand wind behavior correctly and to get the wind predictions right. Equation 2.6 shows the available power in the wind,

$$P_w = \frac{1}{2} \cdot \rho \cdot A \cdot V^3, \tag{2.6}$$

where P_w is the power in the wind, ρ is the air density, A is the cross sectional area through which the wind speed V passes. P_w is also directly proportional to the cross sectional area A, which is $(\pi/4)\mathrm{D}^2$, where D is the blade diameter. However not all of the power offered by wind can be extracted due to the physical constraints. Maximum theoretical efficiency of a turbine is 59.3 % and is called the *Betz efficiency or Betz Law* (Gilbert, 2004).

2.7 Measured data

Field measurement data is taken from three 2.3 MW Siemens wind turbines (SWT-2.3-93) at hub height of 80 meters with base foundations at 420 meters above mean sea level (msl). The turbines were installed at Nygårdsfjell wind farm during the fall of 2005. The wind turbines along with other sensors are equipped with two anemometers on the nacelle; a KK-electronics with thermostat controlled heating element set as the primary anemometer and an NRG IceFree3 set as the secondary. The sensor arrangement is shown in figure 2.6 with KK-electronics anemometer labelled as number 1. It is difficult to expect that the nacelle anemometers give accurate free streaming values of wind speed as specified in IEC standard, but the measurements are sufficient for the detection of significant variations in the wind speed. The wind turbine log files include a wide range of data, including wind speed and direction, ambient temperature, blade pitch, and active power. The data is filtered according to the pitch angle of the turbines, discarding data when pitch angle is above 30 degrees. The data is recorded as 10 minute average values and covered the period from May 2008 to April 2009. There were total $52,560$ data points in one year, out of which $4,066$ data points were found to be either illogical or corrupted. All these data points are filtered out. July lost around 39 % of its data and the remaining valid data made part of the analysis.

Figure 2.7 displays the overall wind speeds and direction at the wind farm. The yearly mean wind speed at the site is 7.45 m/s. Majority of winds are coming from two directions, either East or West having North at 0 degrees. The rest of the scattered winds are relatively low in magnitude. Further investigation is carried out to quantify these winds into two groups. Winds that are equal or higher than 12 m/s are called as "high winds" and the rest are called as "low winds". It is important to know if either of these two groups have specific characteristics and if there is a way to correlate their existence to one of the available parameters such as direction and ambient temperature.

Figure 2.8 divides the overall winds into these two groups and shows the results with corresponding averages of each dataset. The high winds dominantly blow from east and west with almost nothing from any other direction.

Figure 2.6: Anemometers and windvanes on the rear of the turbine nacelle. 1. KK-electronics anemometer.

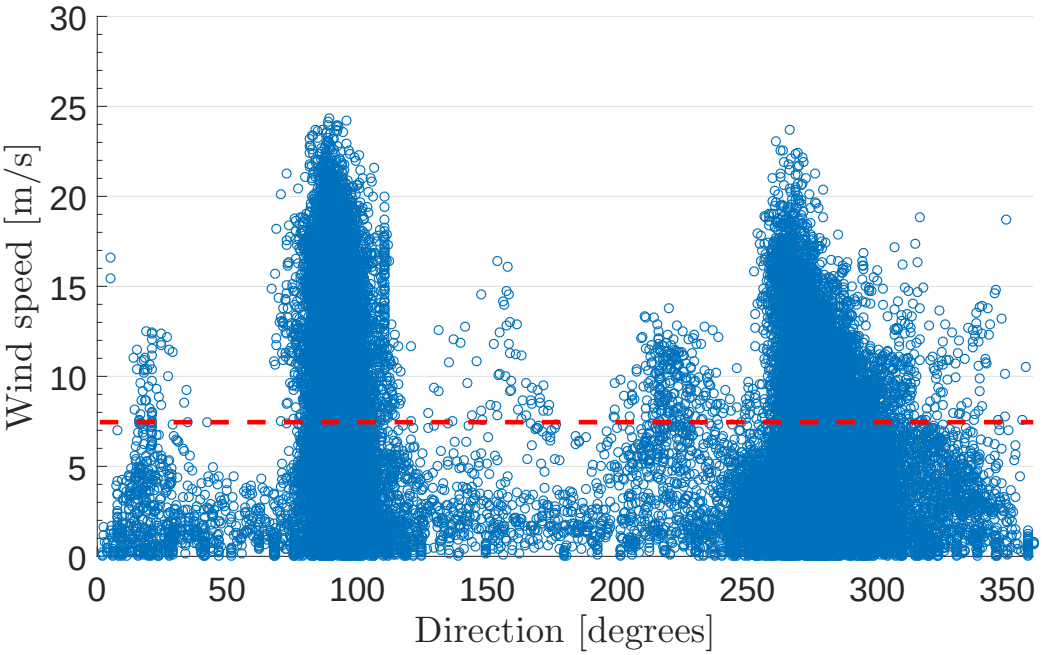

Figure 2.7: Overall wind speed and direction at Nygårdsfjell. Red line indicating mean wind speed of 7.45 m/s.

High winds coming from east are more concentrated and have slightly higher magnitudes than their western counterparts have. These eastern winds have higher occurrences as well over the western winds. The lower winds are spread over larger incoming directions with slightly more concentrated from western side. The mean of high winds is 15.03 m/s whereas mean of low winds is 5.38 m/s. Further analysis is carried out to investigate whether these winds have any specific ambient temperature pattern as well.

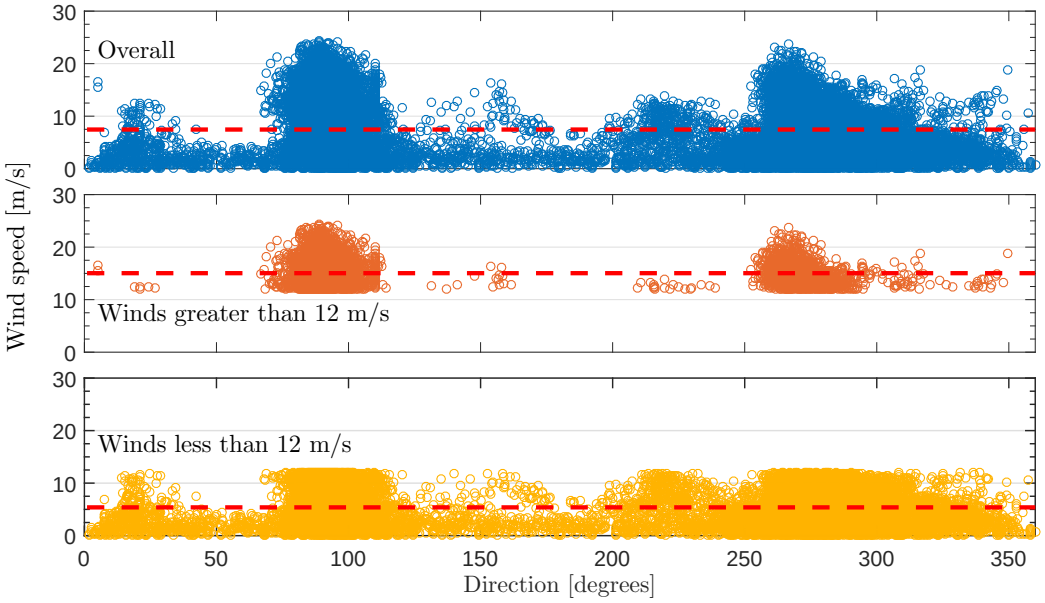

Figure 2.8: Overall winds (mean = 7.45 m/s), Winds equal or greater than 12 m/s (mean = 15.03 m/s) and Winds less than 12 m/s (mean = 5.38 m/s). Red line indicating mean for each group.

Figure 2.9 plots the corresponding ambient temperature values against the high and low winds. It is interesting to note that within the same group of high winds, the temperature profiles shapes differently depending upon the incoming direction of the high winds. When high winds are blowing from East, there are more below freezing point temperature readings as compared to when these winds are coming from West. This indicates the presence of relatively colder winds blowing from eastern direction. The mean ambient temperature during high winds is around -5 °C. Low winds follow slightly scattered pattern compared to high winds and corresponds to relatively higher temperature magnitudes. The mean ambient temperature

during low winds is around 2 °C. The overall annual mean temperature at the site is around 0.80 °C. Figure 2.10 summarizes the wind and its directions for these cases in term of wind roses. The low winds have slightly more contribution from west as compared to the high winds. The overall wind direction is evidently from east of the wind farm.

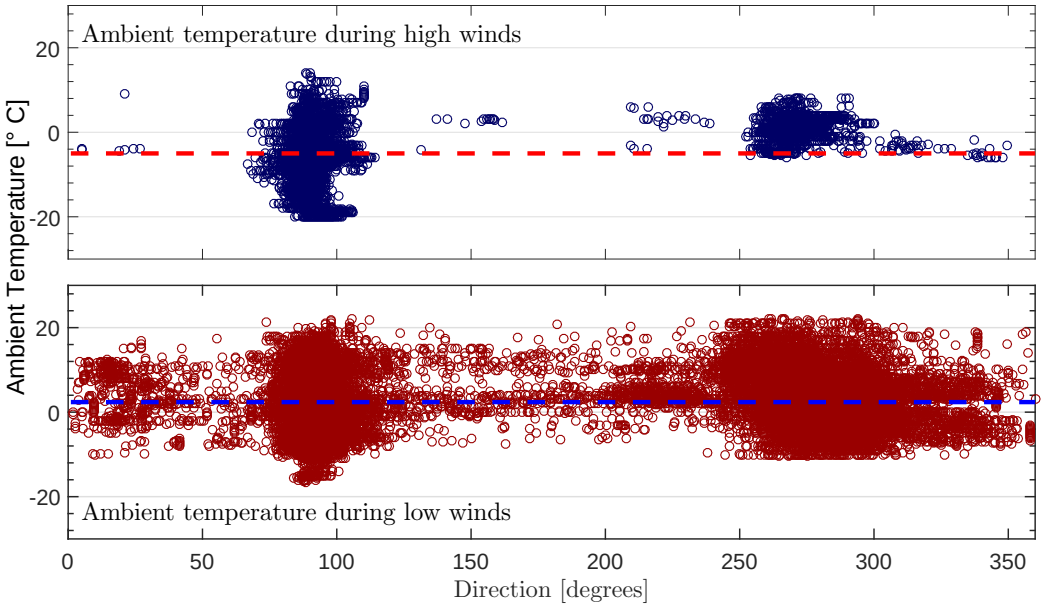

Figure 2.9: Ambient temperature variations, overall mean = 0.80 °C, during high winds −5 °C, during low winds 2 °C. Red and blue lines indicating mean for each group.

It is very appealing to investigate how much these two groups of winds contribute to energy production. Low winds have much higher number of instances than the high winds. Out of total 52, 560 data points over the year, 38, 098 data points correspond to low winds and only 10, 396 data points to high winds. However, the most important factor in power output of any turbine is none other than the magnitude of the wind speed. Figure 2.11 shows the contribution of high and low winds to the measured power along with the original power curve of the turbine. Blue dots correspond to power generated at low winds whereas red dots correspond to the power from high winds. A total of around 7.9 GWh energy is generated during the year, out of which, 52.39 % coming from the low winds and remaining 47.61 % from high winds. Although high winds occurrence is much less than the low winds

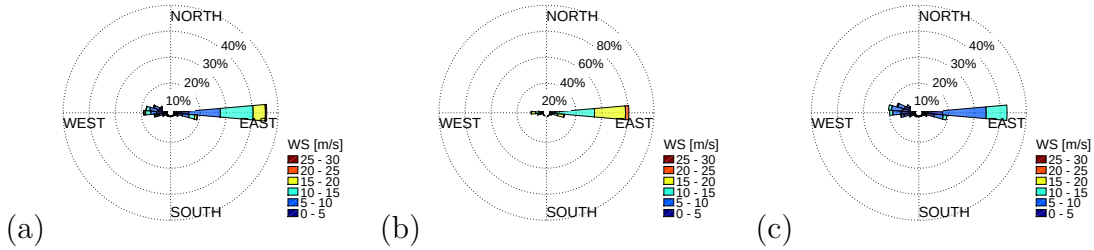

Figure 2.10: Wind Roses: (a) Overall, (b) High winds, (c) Low winds

but their contribution is very much comparable to that of low winds. That may be very important analysis for the wind farm management to keep the wind turbines running especially during high wind events.

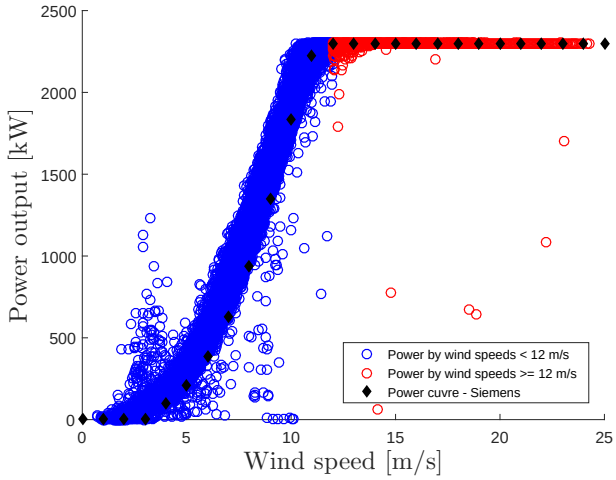

Figure 2.11: Measured power generation of Siemens (SWT-2.3-93) turbine.

Figure 2.12 shows the monthly wind variations over the year while figure 2.13 displaying the monthly wind roses at the site. It is worth noting that during colder periods the wind tends to concentrate more from east and as the warmer periods arrive the wind from west start to contribute more. Monthly wind data also reveals a steady increase in mean wind speed as the winter months approach. Figure 2.14 (a) shows the monthly mean wind speed pattern over the year at Nygårdsfjell along with standard deviation. Especially from December through March, the monthly mean wind speed is at higher magnitudes in comparison to rest of the year. One of the reasons of increased

mean wind speed is credited to the increased number of high wind events that occurs more frequently in colder periods than the warmer periods. Figure 2.14 (b) shows the monthly frequency of high and low wind events throughout the year. The high wind events increases steadily over colder months as compared to their occurrences during warmer months. These events are the main reason of increased mean wind speeds and consequently higher energy output during winter times at Nygårdsfjell. Figure 2.14 (c) shows the ambient temperature records during these high and low wind events. High wind events corresponds to relatively lower ambient temperatures falling well below freezing point between November and March. As discussed earlier, the direction of incoming winds also varies according to season variations and an overview of dominant wind directions through four quarters is given in figure 2.15. Quarter 1 corresponds to May through July, Quarter 2 corresponds to August through October, Quarter 3 corresponds to November through January and Quarter 4 corresponds to February through April. As the colder seasons arrive, the wind is getting more concentrated from East.

The measured data analysis at Nygårdsfjell wind farm showed unique pattern of wind flow. It is safe to state that the site is bi-directional with overwhelming majority of the winds coming from either east or west. The temperature profile strongly indicates the existence of cold winds especially from the east. Further analysis on the presence of cold winds (Katabatic winds) is given in the attached published manuscript, **Paper I**. Moreover, CFD techniques are used to investigate the possibility of modelling wind flow over the complex terrain of Nygårdsfjell. Experimental setup and finding of the project are documented in attached published manuscript **Paper II**. Based on one-year data, it is not possible to say conclusively that the current pattern of winds is a regular occurrence at the Nygårdsfjell wind farm. Nonetheless, it gives better understanding of the local wind flow at the site. It is important to note that the analysis is restricted to the available dataset given by Nordkraft AS.

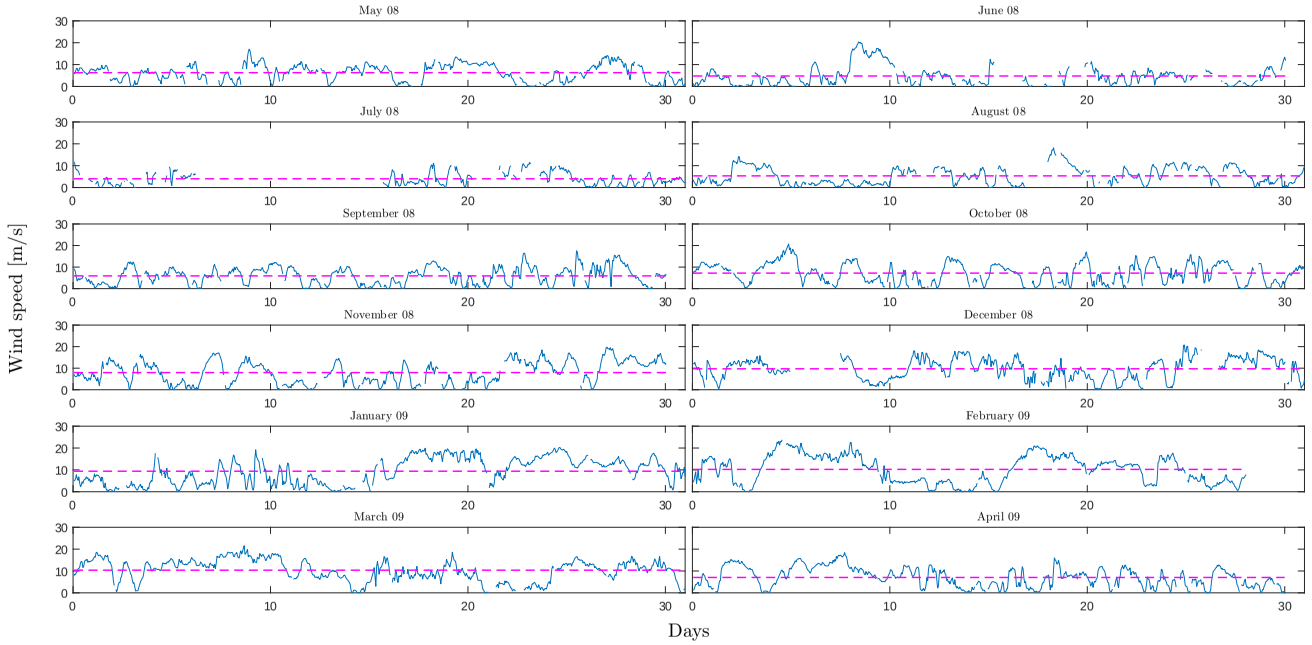

Figure 2.12: Monthly wind speeds at the Nygårdsfjell site for 2008-09. The magenta line indicates monthly mean.

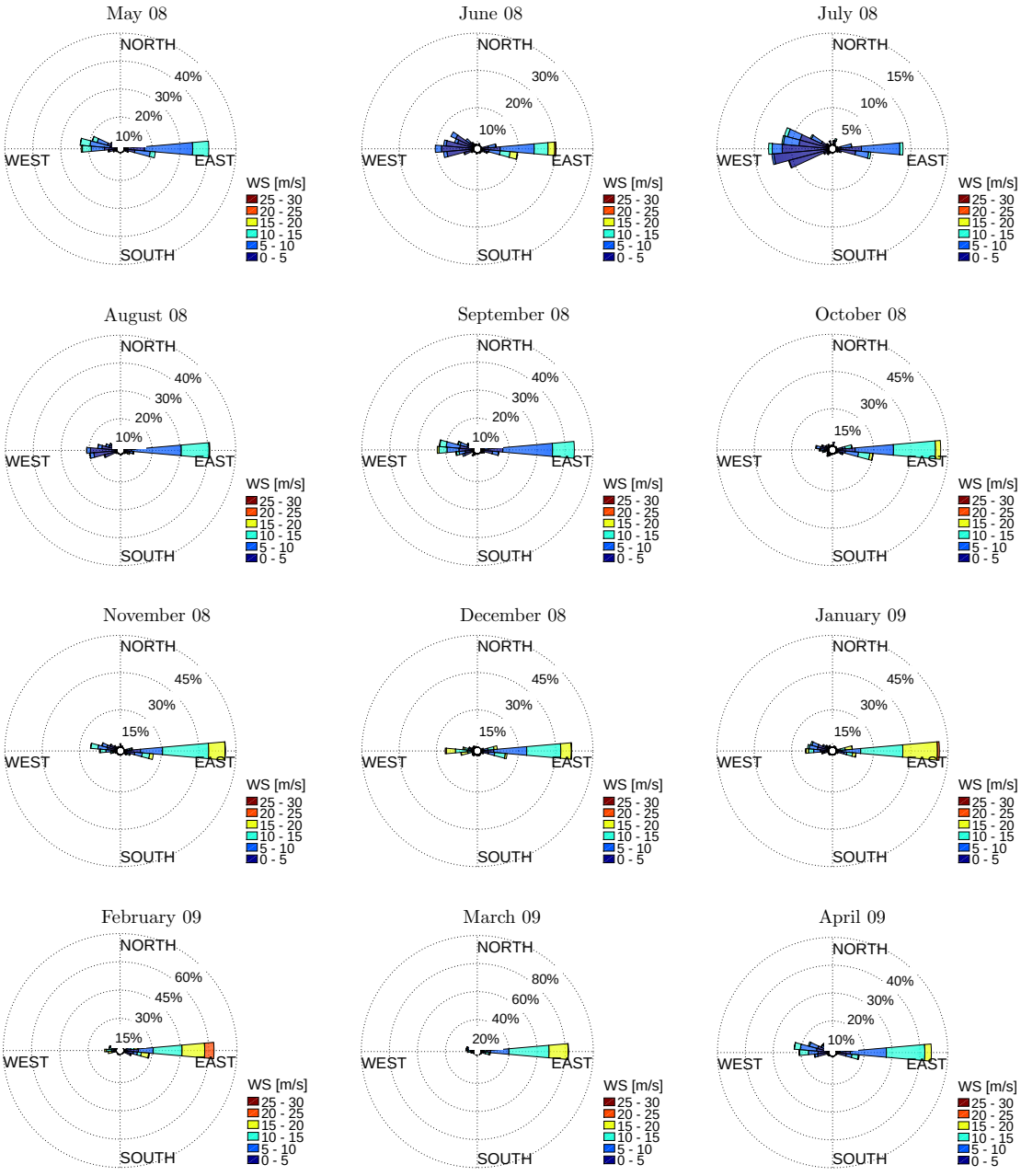

Figure 2.13: Comparing monthly wind roses at Nygårdsfjell site for 2008-09.

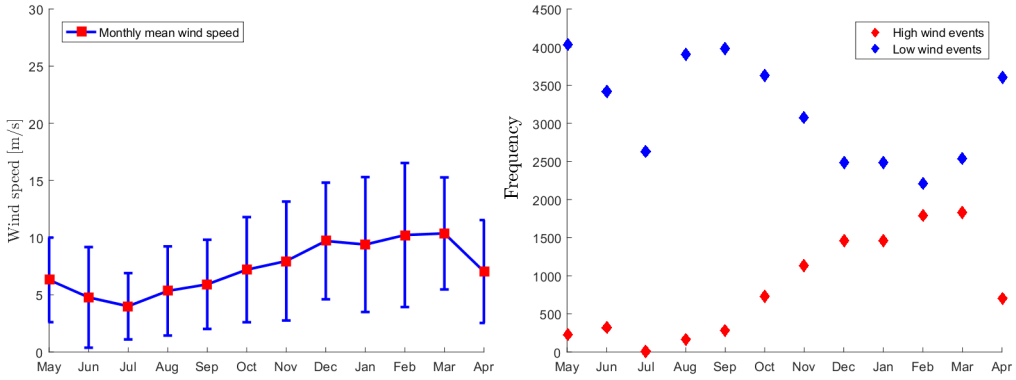

(a)

(b)

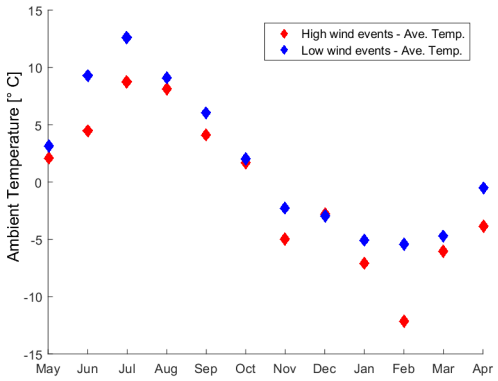

(c)

Figure 2.14: At Nygårdsfjell site for 2008-09: (a) Monthly mean wind speeds with standard deviation (b) Monthly frequency of high and low wind events (c) Monthly mean ambient temperatures during high and low wind events.

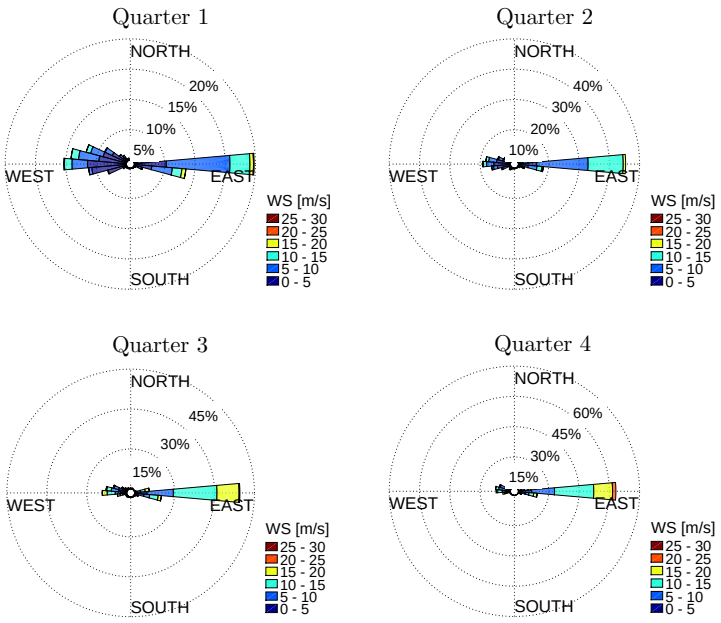

Figure 2.15: Comparing quarterly wind roses at Nygårdsfjell site for 2008-09.

Chapter 3

Weather Research and Forecasting model

Many interacting components and large number of variables and processes make a very complex system called the climate system. Understanding climate system and its behaviour requires obtaining solutions to a large number of governing equations. These governing equations consist of partial differential and integral relationships. There are many processes not completely described by these equations, for instance turbulence. That makes it impossible to obtain general solutions by analytical mathematical methods. Therefore, it is necessary to make certain approximations in both governing equations and the numerical methods to obtain solutions. These approximations are made according to the understanding of the relative importance of various processes represented in the equation. In addition, the computational capacity limits the spatial and temporal resolution available for the physical phenomenon in the numerical model. A meteorological model should represent the whole world but with the resolution constraint, there are processes that cannot be explicitly presented in the model. All these smaller processes must be parameterized. The most successful meteorological models work on a hierarchy of models that deals with isolated physical processes in climate system. The complete model provide the best possible estimation of climate change on very detailed regional basis (Houghton and Organization, 2002).

Weather Research and Forecasting model (WRF) of the Advanced Research WRF solver is a widely used mesoscale model developed by the National Centre for Atmospheric Research (NCAR). WRF is established as a successor to the well-known NCAR Fifth-Generation Mesoscale model and offers multiple physics options that can be combined in different ways. The options typically range from simple and efficient to sophisticated and more computationally costly. WRF has a wide set of physical parameterizations available for microphysics, radiation (long wave and short wave), cumulus, surface layer, planetary boundary layer, and land surface model. Physical parameterization schemes interact non-linearly with each other and with the dynamical core of the model, and these complex relationships make the interpretation of model deficiencies very challenging. Further parameterization schemes are potential sources of errors. Beside these errors, the numerical solvers are also prune to errors from other sources such as initial and boundary conditions, domains sizes, vertical and horizontal resolution, terrain, vegetation characteristics, nudging and assimilation. Topography also plays a crucial role on the climate of the region. Orographic features may substantially effect the regional climate by influencing the dynamics of the atmospheric circulation and the interaction between the atmosphere and the land (Kapos et al. (2000); Kumar et al. (2008)). On a smaller scale, the local terrain plays a vital role influencing the surrounding atmospheric circulation. The other key parameter is resolution of the simulation domain, which effects the accuracy of the local terrain representation.

3.1 WRF parameterization schemes

Even with the highest model resolution, there will always be physical processes and scales of motion that remain unresolved by the model. These small-scale atmospheric phenomena can be critical on how well the model performs. These unresolved physical processes are represented by parameterization. Molecular level physical processes such as, transfer of radiation through atmosphere, formation of cloud droplets are few examples of the physical processes represented by parameterization. There are other parametrization schemes concerning, land and surface, vegetation, convection, microphysics, radiation, cloud cover, orographic drag, to mention a few. However, it is

not feasible or necessary to include all the available model options for the evaluation in order to get the efficient model configuration (Nossent et al., 2011).

The planetary boundary layer (PBL) is defined as that part of the troposphere that directly get influenced by the presence of the Earth's surface and responds to the surface forcing with a timescale of an hour or less (Stull, 1988). The PBL can be as shallow as few tens of meters and as deep as several kilometers (Yamada and Mellor, 1975). WRF model requires PBL parameterizations to represent the transfer of heat, moisture and momentum between the surface and atmosphere (Gilliam and Pleim, 2010). The wind varies according to the regional pressure differences and it is affected by the surface orographs and stability in the boundary layer. PBL schemes plays an important role in terms of WRF performance particularly for wind energy applications.

3.2 WRF model overview

In this research, WRF V3.7.1 is used. Figure 3.1 shows the simplified model diagram for WRF. It consists of three major parts; input data set (Input), WRF pre-processing system (WPS), and ARW dynamic solver (WRF). External data set consists of geographical and meteorological data for the region of simulations. WPS main responsibility is to use the external data and perform tasks such as; define simulation domain, interpolate terrestrial data to the simulation domain, de-gribbing and interpolate meteorological data from another model to the defined simulation domain. Namelist.wps interacts with all three executables in WPS. Each of three WPS executables read parameters from Namelist.wps. The outputs of WPS are fed into WRF solver, which is the soul component of the entire modelling system. WRF solver is composed of various initialization programs for real-data simulations and numerical integration programs. Real.exe and WRF.exe read parameters from Namelist.input. The output of WRF solver is the resulting dynamic downscaling of reanalysis data labelled as Post-processing. The output is further used for post processing and data visualizations.

As mentioned previously, one of the key responsibilities of WPS is de-gribbing and interpolating meteorological data from another model to the defined simulation domain. In this research work, WRF is initialized with reanalysis data from the European Centre for Medium-Range Weather Forecast (ERA-interim Project ds627.0). It is worth spending sometime on understanding the reanalysis data.

3.3 Re-analysis data

Reanalysis data gives a comprehensive representation of the state of the atmospheric system. Gridded datasets of several atmospheric and oceanic variables are produced by combining observations with a meteorological forecast model. The data set extend over decades covering almost the entire planet with temporal resolution of few hours. It is easier to understand reanalysis data once the process of creating analysis data is comprehended. Meteorological models needs to know the current state of the atmosphere known as initial time in order to produce quality forecasts. To achieve this, observations from various sources and places of the earth are integrated into meteorological models by a method called data assimilation cycle. This is easier said than done. Observations coming from various sources around the world might have very different formats, various errors and missing values as well. All of these are needed to be translated into coherent temporal and spatial resolution. Sophisticated mathematical techniques are developed to integrate all these observations into a coherent format, which can then be used for the initialization of meteorological models. This process is called analysis.

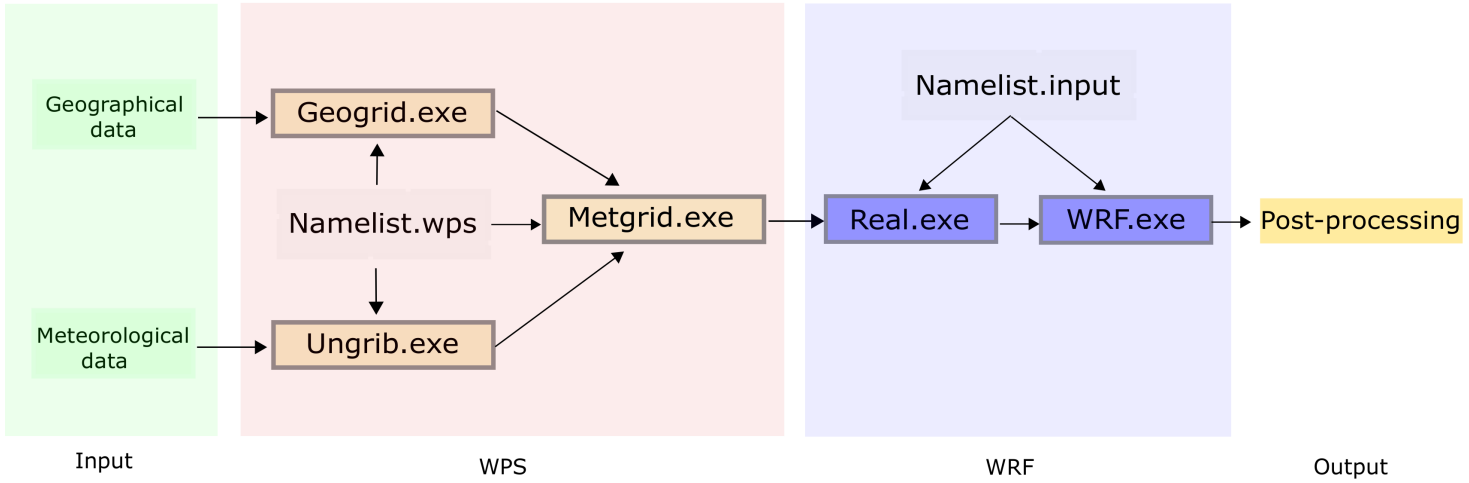

Figure 3.1: Simplified WRF model diagram.

Analyses are produced daily for two to four times and are stored at different locations around the world. Analysis data spanning over decades is very crucial for the atmospheric research since it describes the current state of the atmosphere. However, the process of retrieval is not that straightforward. Over the years with technological advancements, new powerful and efficient meteorological models are developed with refined temporal and spatial resolutions. Many variables have been updated or even extinct from the older data sets, all resulting in inhomogeneity that makes it very difficult to use those analyses in modern day meteorological models. In order to analyse climate change over extended periods, we need to transform the older analysis data into a form that can be integrated into modern metrological models. To achieve this task, few weather forecasting centres around the world decided to revisit their analysis data and transformed it into a format that can be used in modern day meteorological models and this revisited analysis data is called reanalysis. This huge task of producing reanalysis data requires significant technological and financial resources and only handful forecasting centres are capable of doing this. The most known centres are; the National Centre for Environmental Prediction (NCEP-DOE Reanalysis-2, CFSR, and NARR reanalysis) and the European Centre for Medium-Range Weather Forecast (ERA15, ERA40 and ERA-interim reanalyses) (Cóté, 2014; Compo et al., 2011).

3.4 WRF simulation setup at Nygårdsfjell

Figure 3.2 (a) shows location of the Nygårdsfjell wind farm above the Arctic circle whereas figure (b) shows the domain setup of WRF model that surrounds the site. Figure (c) depicts the topography of the proximate region to the site. The input meteorological data as described in the WRF model is taken from the ERA-interim Project ds627.0 data sets from the European Centre for Medium-Range Weather Forecasts, with spatial resolution of approximately 80 km on 60 vertical levels and 6 hours of temporal sampling. Land use and topographical properties are acquired from the US Geological Survey. The parent domain (D01) has a spatial resolution of 18 km x 18 km and the inner nested domains (D02 and D03) have spatial resolutions of 6 km x 6 km and 2 km x 2 km respectively. The vertical resolution of the model

consists of 51 stretched levels. All three domains encompass Nygårdsfjell wind farm with coordinates: Latitude = 68° 30″ 27′; Longitude = 17° 52″ 22′ with interaction protocol feedback from nest to its parent domain. Vertical interpolation at hub-height of 80 meters above ground level is carried out for every model output time stamp, since the heights of the model vertical resolution may vary in time. All the relevant configuration details are given in table 3.1.

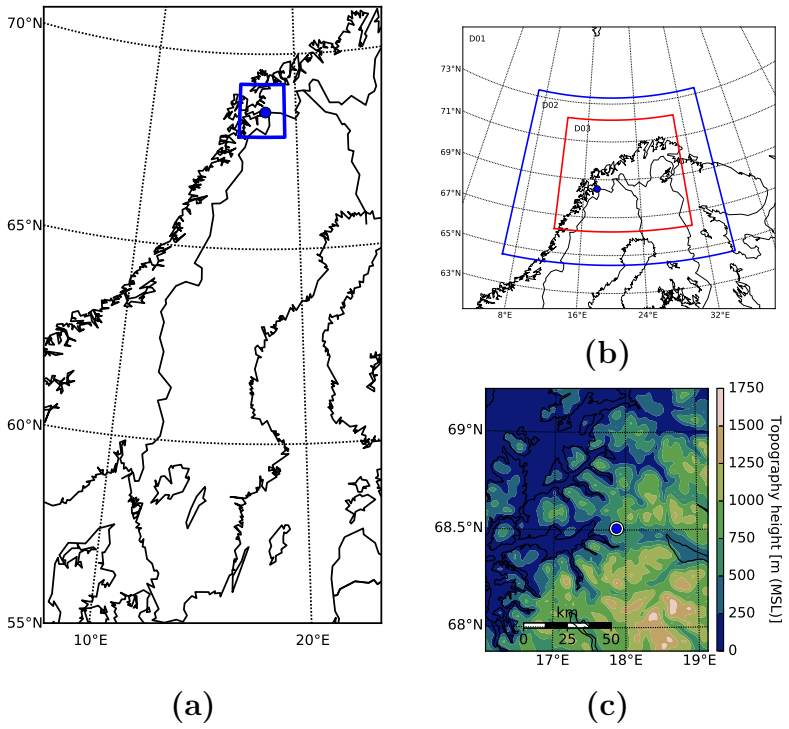

Figure 3.2: Figure (a) gives overview of Nygårdsfjell site. Figure (b) shows WRF domains and (c) shows the topography inside the blue square.

Table 3.1: Summary of the WRF configurations used in this research study

WRF model	WRF V3.7.1
WRF dynamical solver	ARW
Domains	3
2-way nesting	D01: False D02: True D03: True
Domain grid spacing	D01: dx = 18000 m, dy = 18000 m D02: dx = 6000 m, dy = 6000 m D03: dx = 2000 m, dy = 2000 m
Map projection	Polar stereographic
Time step	90 seconds
Adaptive time step	False
Integration scheme	RK3
Advection scheme	5th order advection
Temporal resolution of out-files	10 minutes intervals
Number of vertical levels	51
Microphysics	WSM5
SL scheme	Monin Obhukhov
Land-surface model	Noah Land-Surface model
PBL scheme	MYJ, TKE scheme
Cumulus	Betts-Miller-Janic scheme
Number of soil layers	4
Longwave radiation	New Goddard
Shortwave radiation	New Goddard
Urban physics	Multi-layer BEP scheme
Grid nudging	No grid nudging
Eddy coefficient option	Horizontal Smagorinsky 1st order closure

WRF simulations are run for the period of May 2008 until April 2009 over Nygårdsfjell wind farm. One-and-a-half order turbulent kinetic energy local closure scheme; the Mellor-Yamada-Janjić (MYJ) is selected as PBL scheme along with short and long wave radiation scheme New Goddard. Performance of WRF is evaluated with respect to measurements and available ERA-interim reanalysis data that has a spatial resolution of approximately 80 km and temporal resolution of 6 hours. Both WRF and ERA-interim values are interpolated to turbine location. However, the ERA-interim data values are used at 60 meters height as compared to WRF data values interpolated to 80 meters hub-height. This is done to avoid additional extrapolation losses to already sparse ERA-interim data. From WRF simulations, month of March 2009 is not considered due to large number of missing values in the output.

Modelled values from WRF are available over all three domains as mentioned previously. Domain 3 however has the highest resolution and composed of detailed wind field values as compared to other domains, as shown in figure 3.3. Therefore, domain 3 is used for comparing the WRF wind speeds and directions with ERA-interim and on-site measurements. Figure 3.4 shows yearly comparison of WRF and ERA-interim outputs with those of on-site measurements. WRF seems to follow the on-site wind pattern better than the ERA-interim data. Comparable to measurements, WRF concentrates on mainly two wind directions and matches up with the magnitudes. On the other hand ERA-interim clearly fails to match the wind pattern at Nygårdsfjell both in magnitudes and direction of wind flow. ERA-interim data is almost evenly distributed over 360 degrees with low wind speed magnitudes. Data counts of ERA-interim dataset is understandably low due to its 6 hours temporal resolution.

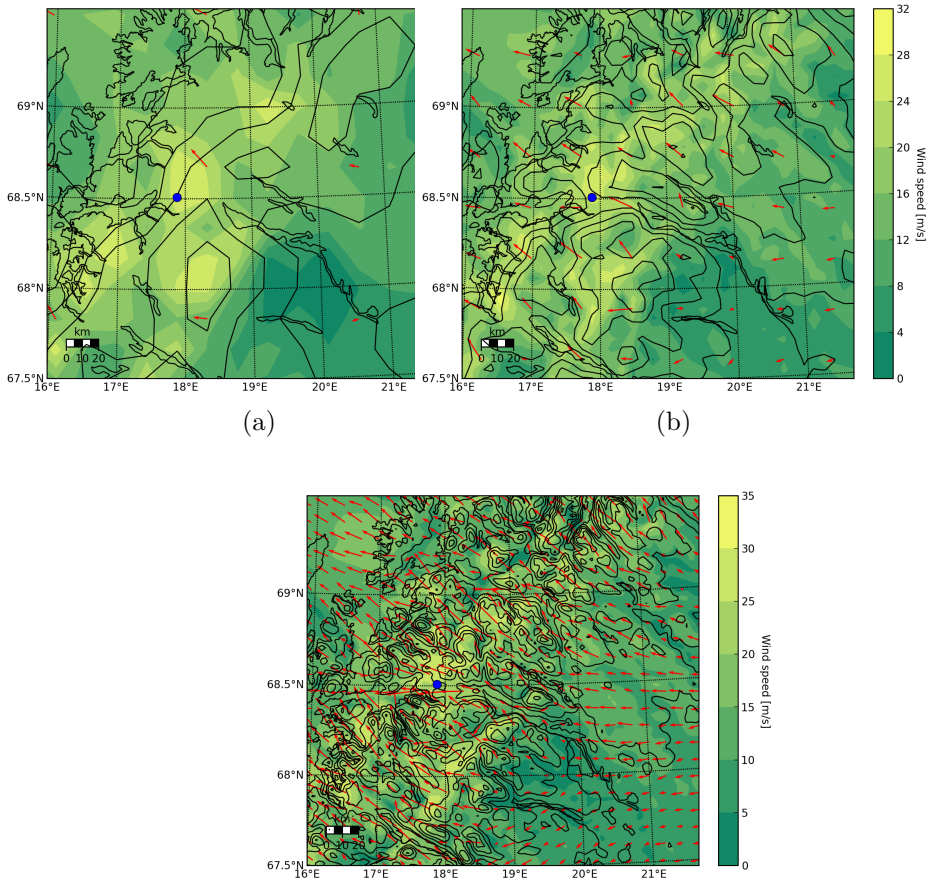

Figure 3.3: WRF wind fields over three domains (80 meters): (a) Domain 01 - 18 km x km (b) Domain 02 - 6 km x km (c) Domain 03 - 2 km x km.

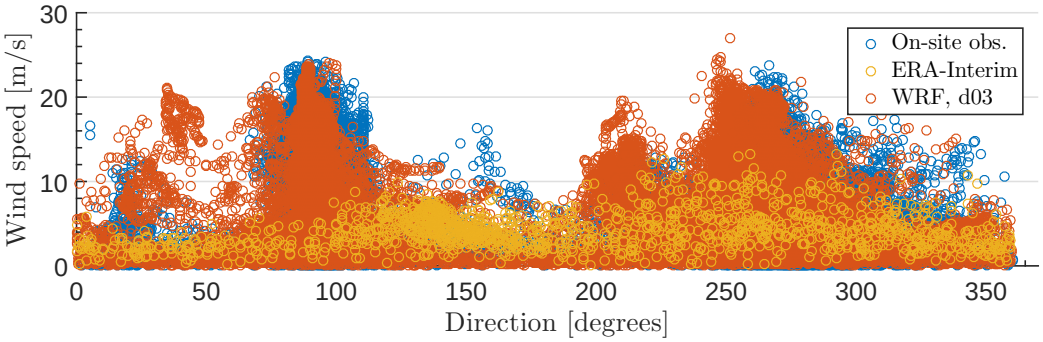

Figure 3.4: Overall wind speed and direction at Nygårdsfjell. Observational, ERA-Interim and WRF domain 3.

Figure 3.5 depicts the wind data separately for all three data sets. ERA-interim data set has a mean value of 4.2 m/s as compared to On-site mean of 7.45 m/s. WRF however has mean value of 7.2 m/s that is closest to the measurements. Overall WRF seems to be pretty good when it comes to mean wind speed. In chapter 2, the measured data is divided into two groups, high winds and low winds. WRF values are divided into these two groups to compare the spread of the modelled values with measurements. Figure 3.6 shows the On-site measurements and WRF values into two groups. WRF seems to perform well in both of the groups, following the directional and magnitude changes of the measured wind fields. WRF has mean value of 15.5 m/s for high winds as compared to measured mean value of 15.1 m/s and WRF mean for low winds 5.46 m/s against measured mean 5.38 m/s. The low wind mean holds more importance than the high wind mean since the turbine would already be generating at its rated power in this case.

Figure 3.7 shows monthly variations of WRF and On-site measurements. WRF model catches the overall major ramp up and down changes in wind speed, the exceptions being few spikes which are not captured by the model. March, as mentioned earlier missing the WRF data values. WRF also performed better in terms of predicting the wind flow direction as compared to ERA-interim data. Figure 3.8 shows quarterly wind roses comparison of modelled values with observations. It can be seen, ERA-interim gives scattered wind direction in contrast to WRF predictions, which are very similar to on-site wind flow directions in all four quarters. Overall, WRF agree with on-site measured pattern of eastern and western winds.

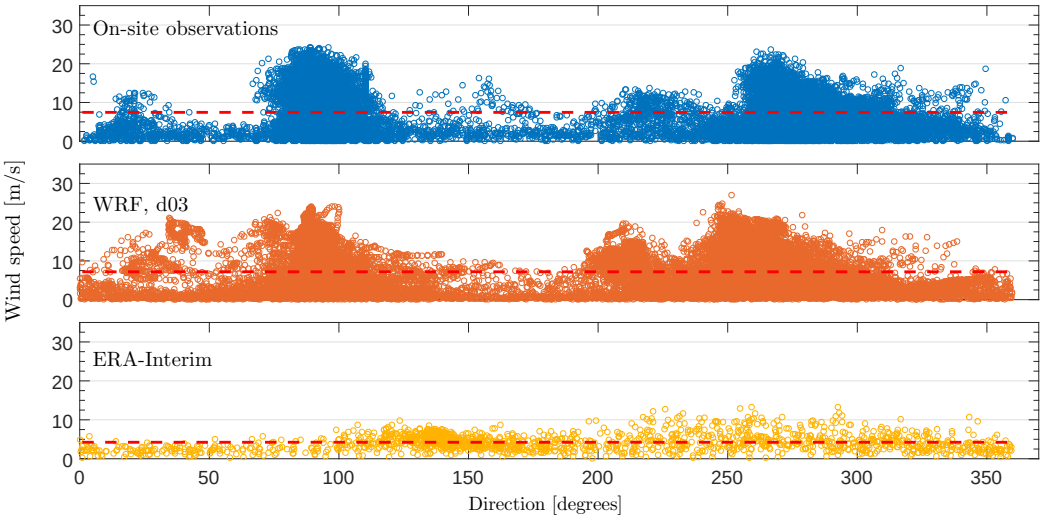

Figure 3.5: Comparison of on site measurements with modelled values at Nygårdsfjell. Red line indicating mean values for each group (Observational 7.45 m/s, ERA-Interim 4.2 m/s and WRF 7.2 m/s).

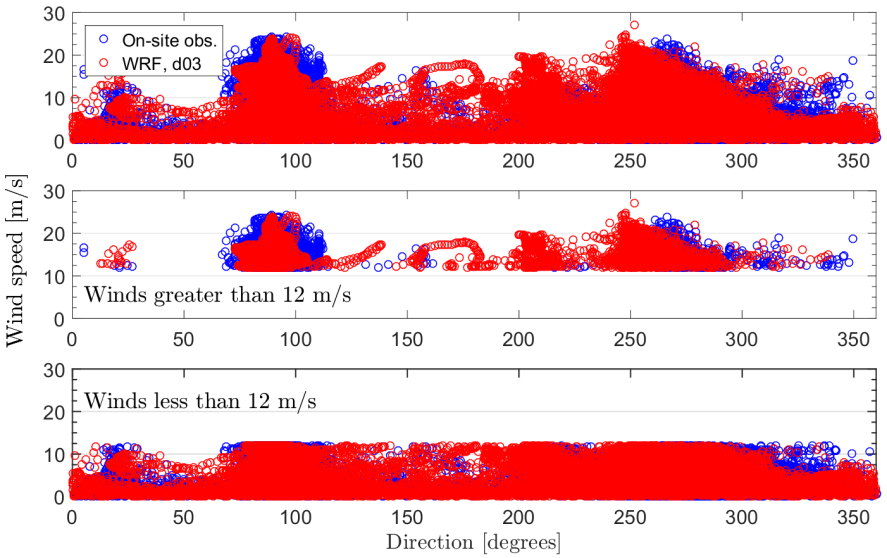

Figure 3.6: Comparison of WRF modelled winds with overall winds, High winds and Low winds.

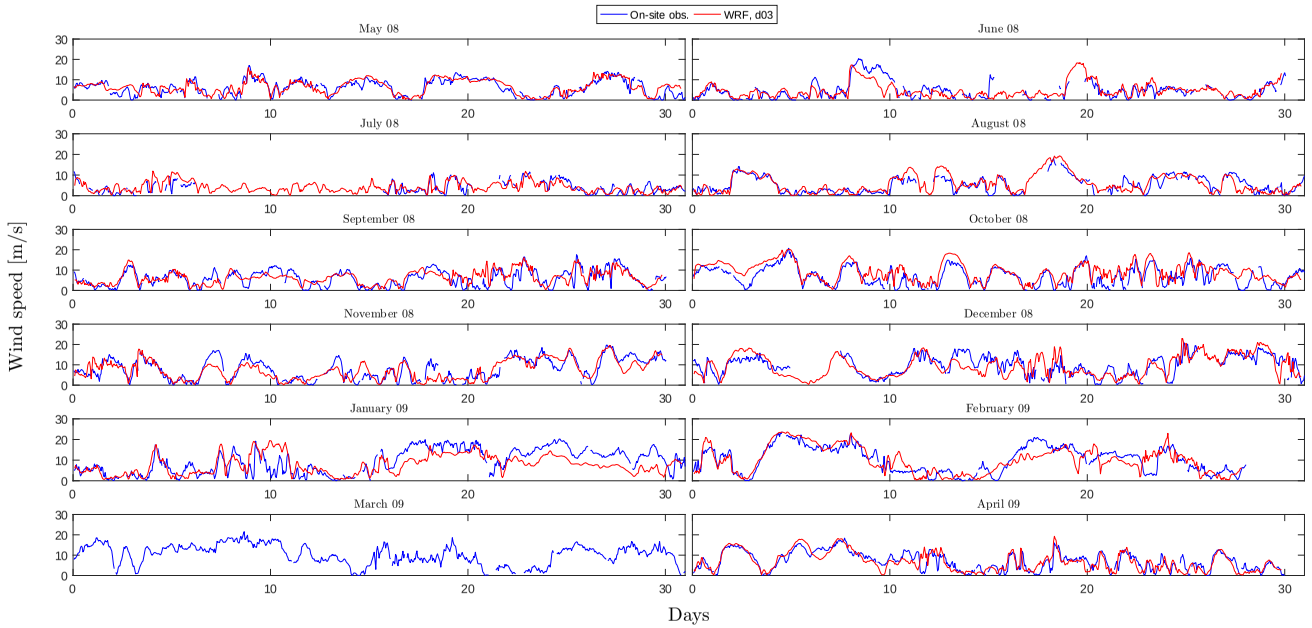

Figure 3.7: Monthly comparison of WRF modelled winds with on site observations.

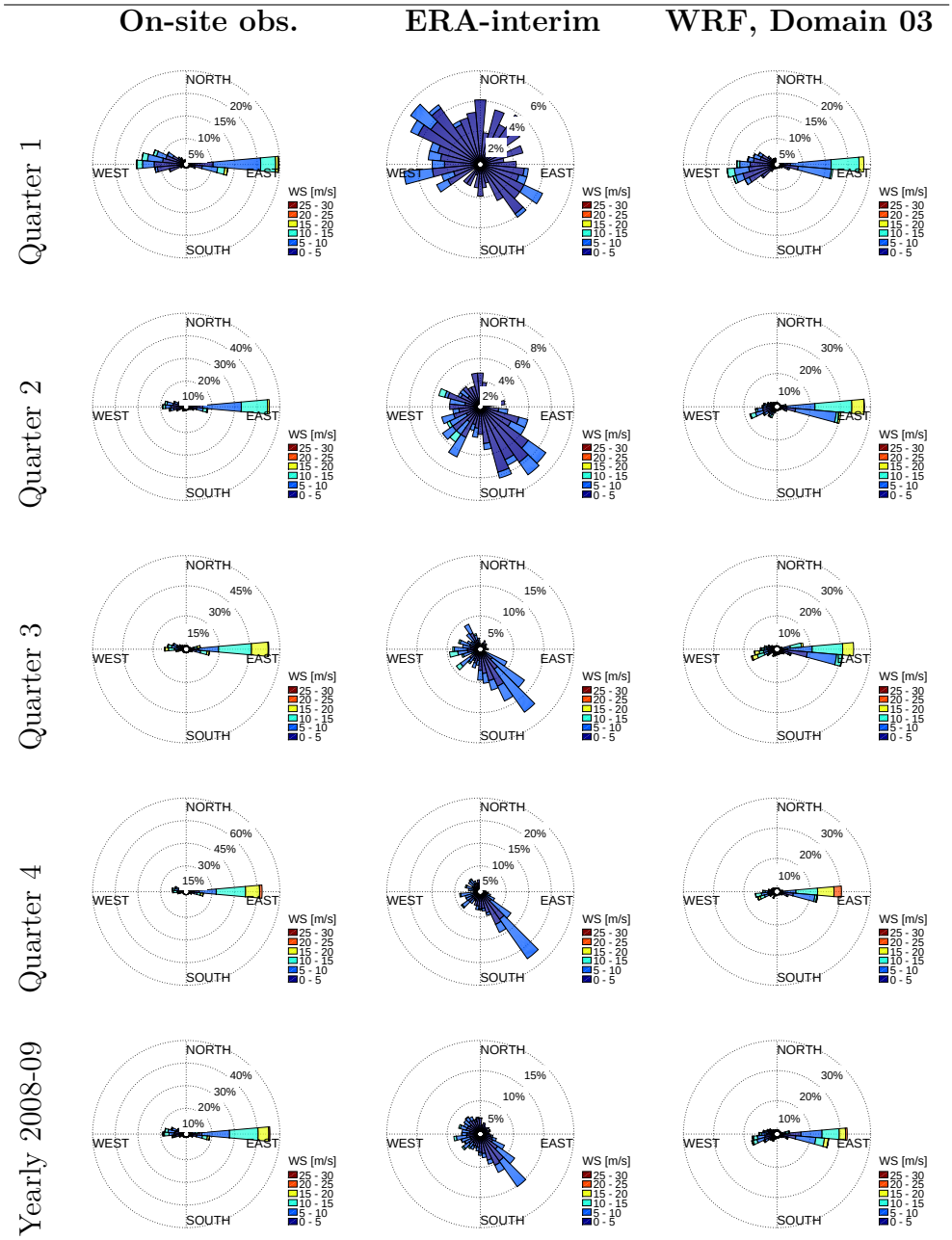

Figure 3.8: Comparisons of wind directions from On-site observations, ERA-interim and WRF domain 3.

Further statistical metrics such as mean, standard deviation, correlation of wind speed and direction as well as root mean square error (RMSE) values are formulated in tables 3.2 and 3.3. The measured mean and standard deviation indicate a well spread data. ERA-interim evidently underestimate the wind resources. On average, ERA-interim underestimate the monthly means by roughly 41 %. That is a big underestimation especially when the wind power output depends on the cube of wind speed. That would translate to roughly 80 % less wind power estimations. WRF domain 3 improve the errors by almost 35 % and on average, under/over estimates the measured values by only 6 %. This is a significant improvement from ERA-interim values. Overall WRF domain 3 performs better along with domain 2 in terms of correlations. However, there are few entries of RMSE where domain 2 performed better than domain 3. This is a bit unexpected since domain 2 has coarser resolution as compared to domain 3. Similar trends were reported by (Passner and Knapp, 2008) and (Blæsterdalen, 2016), where identical domain resolution setup gave better bias results for largest domain rather than the domain with highest resolution. They also reported simulation results from the coarsest domain provided the highest correlation coefficients for temperature. Another study reported that refining the resolution from 30 km to 10 km does not make a significant difference in outputs; citing one of the reasons is the inability of the land use data to capture the Norwegian vegetation in high detail (Heikkilä et al., 2011). Overall, domain 3 and 2 performs better for the discussed parameters as compared to domain 1. Figure 3.9 summarizes the variations of these parameters along with monthly mean wind speeds.

Table 3.2: Comparison between monthly mean and standard deviations of On-site, ERA-interim, WRF-D01, WRF-D02 and WRF-D03 data. Temporal resolution of ERA-interim is 6 hours whereas rest of the data is 10 minutes average.

	On-Site		ERA-I.		WRF, D01		WRF, D02		WRF, D03	
Month	$\bar{x}$	s	$\bar{x}_{ERA}$	s_{ERA}	$\bar{x}_{D01}$	s_{D01}	$\bar{x}_{D02}$	s_{D02}	$\bar{x}_{D03}$	s_{D03}
May	6.2	3.7	3.6	1.9	5.4	3.4	6.4	3.8	6.4	3.4
June	4.8	4.4	2.8	1.6	3.4	3.2	4	3.8	4.6	3.6
July	4.1	2.9	2.7	1.2	2.9	2.3	3.4	2.6	4.1	2.4
August	5.3	3.9	3.1	1.4	4.4	3.7	5.6	4.8	5.8	4.4
September	5.8	3.9	3.8	2.2	5.1	3.5	6.3	3.5	6.2	3.3
October	7.1	4.6	4.6	1.8	7.6	3.8	9.4	4.4	9.1	4.4
November	7.9	5.2	4.6	1.8	6.1	4.1	7.6	4.9	7.3	4.6
December	9.7	5.1	5.8	2.6	8.2	5.2	9.5	5.2	9.3	5.2
January	9.4	5.9	5.6	2.1	7.7	4.5	9.1	5.6	9.1	5.4
February	10.2	6.3	5.1	2.2	9.1	5.8	10.5	6.6	10.1	6.4
March	10.3	4.9	4.6	1.9	-	-	-	-	-	-
April	7	4.5	4.2	2.1	5.3	4.1	6.7	4.9	6.8	4.6

Table 3.3: Correlation coefficients and RMSE between On-site obs. and WRF domains.

		WRF, D01	**WRF, D02**	**WRF, D03**
May	Correlation wind speed	0.815	0.763	0.776
	Correlation wind dir.	0.952	0.942	0.939
	RMSE wind speed	48.41	23.37	21.88
June	Correlation wind speed	0.676	0.725	0.703
	Correlation wind dir.	0.903	0.903	0.917
	RMSE wind speed	81.56	47.74	8.26
July	Correlation wind speed	0.687	0.587	0.585
	Correlation wind dir.	0.898	0.911	0.934
	RMSE wind speed	40.73	11.43	13.30

Table 3.3: Correlation coefficients and RMSE between On-site obs. and WRF domains.

		WRF, D01	**WRF, D02**	**WRF, D03**
August	Correlation wind speed	0.766	0.818	0.811
	Correlation wind dir.	0.914	0.891	0.915
	RMSE wind speed	68.75	8.25	20.42
September	Correlation wind speed	0.544	0.620	0.616
	Correlation wind dir.	0.941	0.944	0.946
	RMSE wind speed	46.55	32.36	27.92
October	Correlation wind speed	0.582	0.705	0.719
	Correlation wind dir.	0.913	0.925	0.922
	RMSE wind speed	43.92	159.69	140.61
November	Correlation wind speed	0.713	0.763	0.757
	Correlation wind dir.	0.907	0.904	0.902
	RMSE wind speed	114.55	10.11	26.74
December	Correlation wind speed	0.565	0.649	0.661
	Correlation wind dir.	0.962	0.966	0.968
	RMSE wind speed	76.33	7.42	12.02
January	Correlation wind speed	0.566	0.715	0.710
	Correlation wind dir.	0.631	0.645	0.645
	RMSE wind speed	102.55	6.8	12.72
February	Correlation wind speed	0.723	0.794	0.789
	Correlation wind dir.	0.922	0.906	0.9066
	RMSE wind speed	74.4	19.4	8.8
March	Correlation wind speed	-	-	-
	Correlation wind dir.	-	-	-
	RMSE wind speed	-	-	-

Table 3.3: Correlation coefficients and RMSE between On-site obs. and WRF domains.

		WRF, D01	**WRF, D02**	**WRF, D03**
April	Correlation wind speed	0.732	0.797	0.793
	Correlation wind dir.	0.952	0.944	0.947
	RMSE wind speed	108.07	21.34	16.56

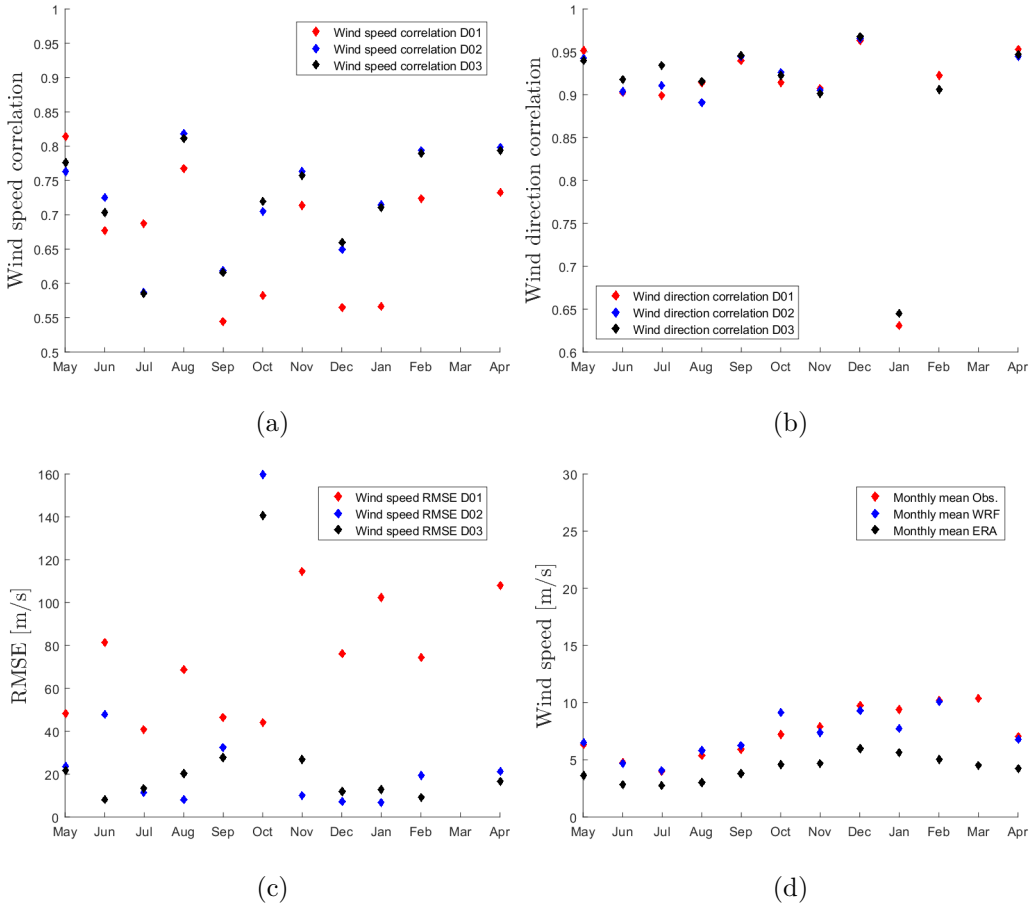

Figure 3.9: Monthly correlations, RMSE and mean wind speed at Nygårdsfjell site for 2008-09: (a) Monthly wind speed correlations for three domains (b) Monthly wind direction correlations for three domains (c) Monthly RMSE variations for three domains (d) Monthly mean wind speed comparison.

3.5 High wind cases at Nygårdsfjell

Three high wind cases are selected from the data set to compare performance of three more PBL schemes. The motivation is to find the best performing PBL scheme for Nygårdsfjell area. The cases are selected from different seasons in an attempt to take into account the seasonal variations. Total four PBL schemes are compared: including two first-order non-local closure schemes YSU (see Hong et al., 2006) and ACM2 (see Pleim, 2007), and two one-and-a-half order local closure turbulent kinetic energy schemes MYJ (see Janijc, 1990) and BouLac (see Bougeault and Lacarrere, 1989). Further, MYJ and BouLac are modelled with short and long wave radiation scheme, Community Atmosphere Model (CAM). YSU and ACM2 could not be tested with CAM due to incompatibilities of these parameterization schemes.

Simulations are run for the selected high wind days in June 2008, October 2008 and February 2009. Appropriate changes are made to WRF configurations, earlier mentioned by table 3.1, for the simulations. The high wind events involved wind speeds between 12 - 24 m/s and one of them lasted up to four and a half days uninterruptedly. Shin and Hong (2011) stated major differences among the PBL schemes stating: In PBL parameterization, prognostic mean variables are used to parameterize the sub grid-scale turbulent fluxes through vertical diffusion equations. YSU and ACM2 are classified as first-order closure schemes since they do not require any additional prognostic equations to express the effects of the turbulence on mean variables. For the convective boundary layer, both schemes are based on the K profile in determining the diffusivity within the boundary layer, while diffusivity is a function of local wind shear and local Richardson number in the free atmosphere. In addition to the simple local diffusion, both the YSU and ACM2 schemes consider non-local mixing by convective large eddies. One-an-a-half order closure schemes, MYJ and BouLac are classified as TKE closure schemes and they require one additional prognostic equation of the TKE. Local TKE closure schemes apply the local mixing with the local diffusivity from the lowest to the highest vertical level for both convective boundary layer and stable boundary layer, and there is no separation between the PBL and the free atmosphere mixing. Thus, the entrainment is represented using the computed diffusivity from the prognostic TKE near the PBL top.

The simulation results for the wind speed and direction for the selected months of June 2008, October 2008 and February 2009 are presented in figures 3.10 and 3.11. For wind speed predictions, all the PBL schemes perform quite similar. They were successful in following the general ramp up and down pattern of the observed wind speed with some under-over estimations. For wind direction predictions, all PBL schemes did exceptionally well in all seasons with minor discrepancies during initial and finishing stages of high wind events. Selected statistical parameters are sorted according to RMSE values in Table 3.4. YSU-GOD-GOD has lowest RMSE and good correlation values for October case. For February case, MYJ-CAM-CAM have the least RMSE values. For June both YSU-GOD-GOD and MYJ-CAM-CAM performed similar. As it can be seen that the RMSE values are very close to each other and it is important to know whether these differences are statistically significant or not. Table 3.5 state statistical significance of RMSEs of each of the compared PBL schemes according to the t-test with 95 % confidence level on mean square errors. Although only few RMSEs are found to be non significant, the limited test cases do not allow to conclusively determine which scheme is better.

However, these meso-scale winds along with another set are used as input to micro-scale modelling tool WindSim to evaluate the performance of coupled model. Choice of methods and results are mention in the attached published **Paper III**.

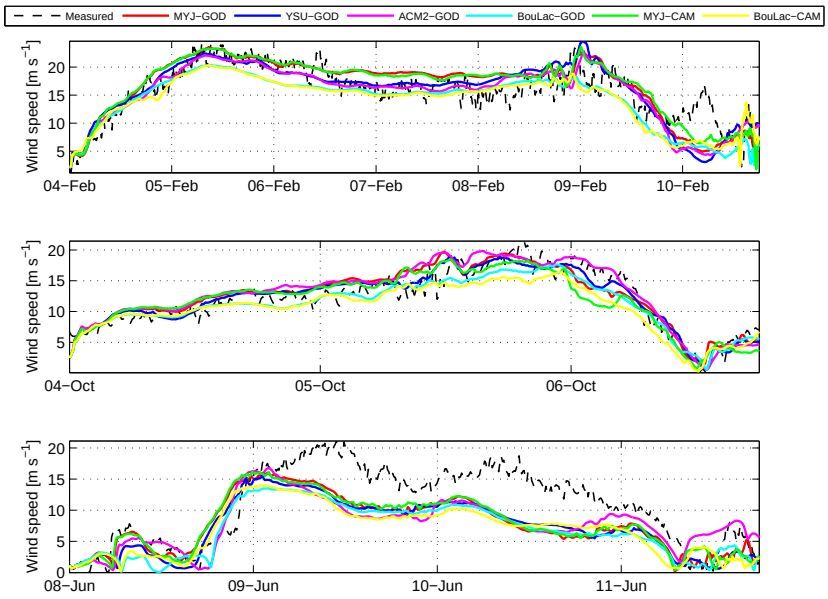

Figure 3.10: Wind speed comparison of four PBL schemes

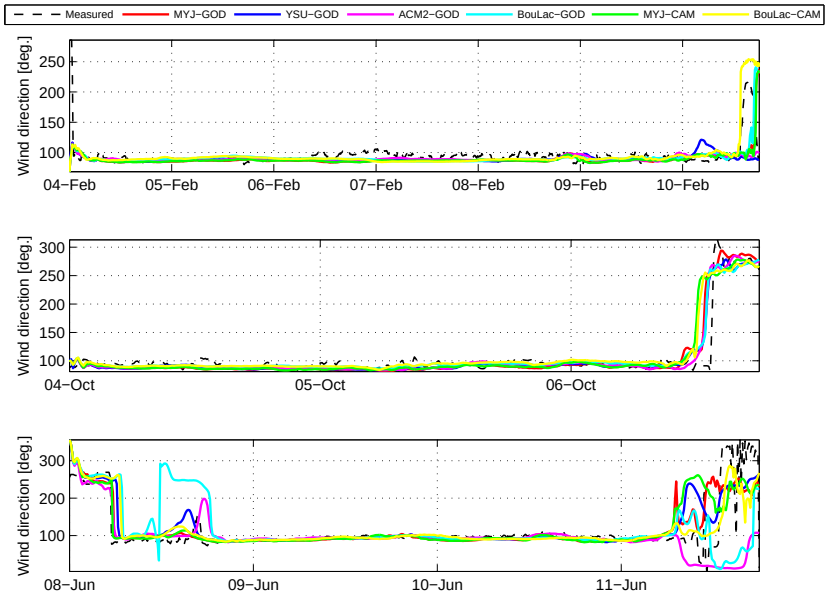

Figure 3.11: Wind direction comparison of four PBL schemes

Table 3.4: PBL schemes performance eveluation with respect to RMSE, Correlation and Bias

PBL-Scheme	**Radiation**	WS_RMSE	WS_Bias	WD_Bias	STDE_WS	WS_Corr.	WD_Corr.	Month
YSU	GOD-GOD	1.4911	0.226	2.3044	1.473873539	0.9485	0.9404	October
BouLac	GOD-GOD	1.6847	0.7751	0.3286	1.495805495	0.951	0.9355	October
ACM2	GOD-GOD	1.8929	0.9933	2.0236	1.611342769	0.9457	0.9359	October
MYJ	GOD-GOD	1.9164	0.5733	1.9886	1.828637763	0.9208	0.9294	October
MYJ	CAM-CAM	2.2095	0.011	1.1305	2.209472618	0.8836	0.8732	October
BouLac	CAM-CAM	2.3068	1.3461	2.4633	1.873323525	0.92	0.8866	October
MYJ	CAM-CAM	2.725	1.1422	6.5003	2.474066321	0.8743	0.1468	February
ACM2	GOD-GOD	2.8635	0.2221	5.3012	2.854873699	0.8278	0.132	February
BouLac	GOD-GOD	2.9661	1.5847	3.7218	2.507284411	0.856	0.2113	February
BouLac	CAM-CAM	2.9802	1.6318	0.5045	2.493756363	0.8506	0.6194	February
MYJ	GOD-GOD	2.9903	0.9684	6.321	2.829151026	0.8499	0.1731	February
YSU	GOD-GOD	3.1098	0.2918	5.6254	3.096079586	0.8059	0.0031	February
YSU	GOD-GOD	4.6598	3.4699	5.7653	3.1102299	0.8716	0.7614	June
MYJ	CAM-CAM	4.6681	2.9694	4.0718	3.601919107	0.8071	0.6789	June
MYJ	GOD-GOD	4.7004	3.0329	2.0714	3.590999547	0.8102	0.7635	June
ACM2	GOD-GOD	4.8242	2.8833	15.9812	3.867749572	0.7811	0.3043	June
BouLac	GOD-GOD	5.0664	4.0138	4.4247	3.091572176	0.8848	0.2214	June
BouLac	CAM-CAM	5.3066	3.9485	1.7795	3.545328096	0.8289	0.7903	June

Table 3.5: Statistical significant test results (t-test) by taking 95 % confidence level on mean square errors (MSE) of the two schemes with respect to measurements.

PBL-Scheme I	**PBL-Scheme II**	**Month**	**Statistical significance**
YSU GOD	BouLac GOD	October	Yes
YSU GOD	ACM2 GOD	October	Yes
YSU GOD	MYJ GOD	October	Yes
BouLac GOD	ACM2 GOD	October	Yes
BouLac GOD	MYJ GOD	October	Yes
ACM2 GOD	MYJ GOD	October	No
YSU GOD	BouLac GOD	February	Yes
YSU GOD	ACM2 GOD	February	Yes
YSU GOD	MYJ GOD	February	Yes
BouLac GOD	ACM2 GOD	February	No
BouLac GOD	MYJ GOD	February	No
ACM2 GOD	MYJ GOD	February	Yes
YSU GOD	BouLac GOD	June	Yes
YSU GOD	ACM2 GOD	June	Yes
YSU GOD	MYJ GOD	June	No
BouLac GOD	ACM2 GOD	June	Yes
BouLac GOD	MYJ GOD	June	Yes
ACM2 GOD	MYJ GOD	June	Yes
BouLac CAM	MYJ CAM	October	No
BouLac CAM	MYJ CAM	February	Yes
BouLac CAM	MYJ CAM	June	Yes

Chapter 4

Publications

Chapter 5

Conclusion and future work

5.1 Conclusion

The research conducted in this thesis extends the current understanding of the wind behaviour over complex terrain and modelling possibilities using available numerical tools. Nygårdsfjell wind farm, situated above the Arctic circle, is the central location for the research activities. Nygårdsfjell wind farm have been reported to experience high winds particularly during cold seasons. However, nothing had been quantified before. Existence of high winds and its pattern is established with analysis of measured data at the wind farm. The influence of local terrain is comprehended by the use of CFD models showing that the wind turbine placements truly capitalize the local flow acceleration resulting in higher power generation. Further, two sets of meso-scale winds are used in CFD based micro-scale modelling tool - WindSim to evaluate the performance of coupling model. The coupling model showed promising improvements in predicting wind speed at the site. A preliminary wind resource assessment method is tested by using nearby measured data sites. However, the conditions and location of the test site strongly disagree with the complex terrain at Nygårdsfjell wind farm. Thus, we cannot adopt the outcomes of this research directly into our main research question. Results from individual projects are given in the following.

Wind flow over Nygårdsfjell - There were total of 185 high wind events detected consisting of 1737 hours during the observation period May 2008 until April 2009. Out of these 1737 hours of high winds, 269 hours occurred during May 2008 until October 2008 and 1468 hours occurred during November 2008 until April 2009 that is 84.5 % of total high winds hours. That shows the majority of high winds events occurring during the colder periods. The overwhelming majority of these high winds are coming from east of the wind farm. The analysis also established the existence of bi-directional - eastern and western wind flows at Nygårdsfjell wind farm with almost negligible winds coming from elsewhere.

Numerical modelling of wind fields over Nygårdsfjell - Numerical simulations over a real complex terrain in north Norway have been performed in a suite of RANS by means of three different turbulence models. Overall, the shear stress transport model gives good simulation results that qualitatively agreed with the existence of rich wind resources at the wind farm site. It has been concluded that local terrain plays a vital role in directing the wind over the hill and eventually into the Ofotfjord in the west. The wind turbine location at the top of the hill is appropriate in the sense of local flow acceleration; consequently, increasing the wind energy production.

Meso-micro scale coupling of wind fields over Nygårdsfjell - The proposed coupled model achieved improvements in wind speed predictions. The meso-micro scale based WRF-WindSim coupling model showed a better solution for predicting the wind flow over the complex terrain of Nygårdsfjell than the MERRA-WindSim coupling for the given data set. The ability of WRF to solve wind fields by taking into account the physical processes and atmospheric conditions compliments the ability of WindSim to perform micro-scale modelling of the complex terrain.

Wind resource assessment - The proposed method offers a potentially practical and resource friendly way of conducting a preliminary assessment of wind resources at a remote site. This technique is tested at a single site on limited dataset in West Texas USA. The findings of the project cannot be adopted directly to thesis focus due to strong disagreement with the complex terrain at Nygårdsfjell wind park.

5.2 Future work

There are number of projects, which can follow this research work. Few of the most important projects are given in the following.

A manuscript is to be submitted regarding the performance analysis of dynamical downscaling of ERA-interim reanalysis using Weather Research and Forecast (WRF) model at two complex sites in North Norway. The study focuses on investigating performance of WRF in terms of its ability to match the field measurements, improvements in Era-interim reanalysis and whether or not increasing the domain resolution of WRF will add significant value to downscaled output. The WRF outputs are compared with field measurements and ERA-interim reanalysis for the period of one year at both sites. Correlation, Bias and RMSE are the benchmark statistics evaluating WRF performance.

During summer of 2015, field measurement campaign was conducted at Nygårdsfjell wind farm using Light Detection and Ranging (LIDAR) with collaboration of Nordkraft AS. Due to the time limitation, this project could not be included in this research work. LIDAR gives wind field values at various heights simultaneously which is very interesting for the detection of different suspected layers of wind flow over Nygårdsfjell wind farm. One possibility is to use WRF modeling to simulate the scenario and evaluate the performance of PBL schemes.

In present research, WRF is used with reanalysis data to learn about the wind behaviour over complex terrain. The next step is to run WRF for predicting the wind flow for the coming 6 - 36 hours at the site of interest. Close collaboration among industry, energy and climate research group and the supercomputing facility at UiT - The Arctic University of Norway is a prerequisite for materializing this project.

Evaluation of aerodynamic loads over wind turbines due to high winds in north Norway is another potential project that can benefit the wind farm operations and maintenance. WRF simulated results along with measured data can be used for this analysis. FAST an aeroelastic simulator developed by the National Renewable Energy Laboratory is capable of predicting the

aerodynamics loads of two- and three-bladed horizontal-axis wind turbines. AeroDyn module can compute the aerodynamic loads over the wind turbine based on the Blade Element Momentum theory. ElastoDyn uses Kane's method to set up equations of motion, which are solved by numerical integration. This project will benefit long term planning with respect to wind farm operations and maintenance.

One of the projects, combining all the previous research results and skills is to create a wind farm simulator that can give short-term prognoses for energy production, turbine loads and turbine lifetimes.

List of Figures

List of Tables

Bibliography

Philip S Anderson, Russell S Ladkin, and Ian A Renfrew. An autonomous doppler sodar wind profiling system. Journal of Atmospheric and Oceanic Technology, 22(9):1309–1325, 2005.

R Avissar, MD Moran, G Wu, RN Meroney, and RA Pielke. Operating ranges of mesoscale numerical models and meteorological wind tunnels for the simulation of sea and land breezes. Boundary-Layer Meteorology, 50 (1-4):227–275, 1990.

Ian Baring-Gould, Lars Tallhaug, Göran Ronsten, Robert Horbaty, René Cattin, Timo Laakso, Michael Durstewitz, Antoine Lacroix, Esa Peltola, and Tomas Wallenius. Recommendations for wind energy projects in cold climates. Technical report, VTT working papers 151: 61, 2010.

Roger G Barry and Richard J Chorley. Atmosphere, weather and climate. Routledge, 2009.

Torgeir Blæsterdalen. Wind resource assessment using mesoscale modelling. Masters thesis at UiT, 2016.

Philippe Bougeault and P Lacarrere. Parameterization of orography-induced turbulence in a mesobeta–scale model. Monthly Weather Review, 117(8): 1872–1890, 1989.

O Byrkjedal and Erik Berge. The use of WRF for wind resource mapping in Norway. In 9th WRF users' workshop, 2008.

Gilbert P Compo, Jeffrey S Whitaker, Prashant D Sardeshmukh, Nobuki Matsui, Robert J Allan, Xungang Yin, Byron E Gleason, RS Vose, G Rutledge, P Bessemoulin, et al. The twentieth century reanalysis project.

Quarterly Journal of the Royal Meteorological Society, 137(654):1–28, 2011.

Hélène Côté. Faq6 - what is reanalysis? `http://www.ouranos.ca/en/faq/fiche6En.php`, 2014. Last accessed: 2014-02-16.

Judith A Curry and Peter J Webster. Thermodynamics of atmospheres and oceans, volume 65. Academic Press, 1998.

Stefan Emeis. Wind energy meteorology: atmospheric physics for wind power generation. Springer Science & Business Media, 2012.

LL Freris. Meteorological aspects of the utilization of wind as an energy source, 1981.

Ing Robert Gasch and Ing Jochen Twele. The wind. In Wind Power Plants, pages 114–167. Springer, 2012.

Robert Gasch and Jochen Twele. Wind power plants: fundamentals, design, construction and operation. Springer Science & Business Media, 2011.

M Gilbert. Masters, renewable and efficient electric power systems. Wiley-Interscience, John Wiley & Sons, Inc, New Jersey, 75:76, 2004.

Robert C Gilliam and Jonathan E Pleim. Performance assessment of new land surface and planetary boundary layer physics in the WRF-ARW. Journal of Applied Meteorology and Climatology, 49(4):760–774, 2010.

AR Gravdahl, S Rorgemoen, and Morten Thogersen. Power prediction and siting–when the terrain gets rough. In The World Wind Energy Conference and Exhibition, 2002.

Klaus Hansmann. TA Luft: technische Anleitung zur Reinhaltung der Luft. Beck, 1987.

U Heikkilä, A Sandvik, and Asgeir Sorteberg. Dynamical downscaling of ERA-40 in complex terrain using the WRF regional climate model. Climate Dynamics, 37(7-8):1551–1564, 2011.

Matthew Carl Homola. Impacts and causes of icing on wind turbines. Navrik University College Report, 2005.

Song-You Hong, Yign Noh, and Jimy Dudhia. A new vertical diffusion package with an explicit treatment of entrainment processes. Monthly Weather Review, 134(9):2318–2341, 2006.

David D Houghton and World Meteorological Organization. Introduction to climate change: lecture notes for meteorologists. Secretariat of the World Meteorological Organization Geneva, Switzerland, 2002.

Michael F Hutchinson and John C Gallant. Representation of terrain. Geographical information systems, 1:105–124, 1999.

J Janijc. The step-mountain coordinate: physical package. Mon. Weather Rev, 118:1429–1443, 1990.

Valerie Kapos, J Rhind, Mary Edwards, MF Price, C Ravilious, N Butt, et al. Developing a map of the world's mountain forests. Forests in sustainable mountain development: a state of knowledge report for 2000. Task Force on Forests in Sustainable Mountain Development., pages 4–19, 2000.

Jeremy R Krieger, Jing Zhang, David E Atkinson, Xiangdong Zhang, and Martha D Shulski. Sensitivity of WRF model forecasts to different physical parameterizations in the Beaufort sea region. 2009.

P Krogsgaard, BT Madsen, F Zhao, A Karcanias, and B Hamilton. A btm wind report-world market update 2012-international wind energy development-forecast 2013–2017, 2013.

Oliver Krüger, Christina Schrödinger, Antonio Lengwinat, and Christian Oliver Paschereit. Numerical modeling and validation of the wind flow over the lake wannsee. Proceedings of the 6th European Conference on Computational Fluid Dynamics, 20-25 July, Barcelona, Spain, c(Wccm Xi):5217–5228, 2014.

Sujay V Kumar, Christa D Peters-Lidard, Joseph L Eastman, and Wei-Kuo Tao. An integrated high-resolution hydrometeorological modeling testbed using LIS and WRF. Environmental Modelling & Software, 23(2):169–181, 2008.

Timo Laakso, H Holttinen, G Ronsten, L Tallhaug, R Horbaty, I Baring-Gould, A Lacroix, E Peltola, and B Tammelin. State-of-the-art of wind energy in cold climates. IEA annex XIX, 24, 2003.

Antoine Lacroix and James F Manwell. Wind energy: cold weather issues. University of Massachusetts at Amherst, Renewable Energy Laboratory, 2000.

Peter Lancaster and Kestutis Salkauskas. Curve and surface fitting. Academic press, 1986.

Christophe Leclerc and Christian Masson. Abnormally high power output of wind turbine in cold weather: A preliminary study. International Journal of Rotating Machinery, 9(1):23–33, 2003.

David R Legates and Cort J Willmott. Mean seasonal and spatial variability in global surface air temperature. Theoretical and Applied Climatology, 41(1-2):11–21, 1990.

Germanischer Lloyd. Richtlinie für die zertifizierung von windenergieanlagen. Vorschriften und Richtlinien, 2003.

Joel Manning, Jon Woodcock, Jean-François Corbett, Richard Whiting, James Bleeg, Lars Landberg, and Andrew Tindal. Validation and challenges of cfd in complex terrain for real world wind farms. Annual conference of the European Wind Energy Association, (1758), 2011.

Jiri Nossent, Pieter Elsen, and Willy Bauwens. Sobol' sensitivity analysis of a complex environmental model. Environmental Modelling & Software, 26 (12):1515–1525, 2011.

AM Obukhov. Turbulence in an atmosphere with a non-uniform temperature. Boundary-layer meteorology, 2(1):7–29, 1971.

Jeffrey E Passner and David I Knapp. Using wrf-arw data to forecast turbulence at small scales. In Preprints, 13th Conf. on Aviation, Range, and Aerospace Meteorology, New Orleans, LA, Amer. Meteor. Soc. P, volume 3, 2008.

Erik L Petersen, Niels G Mortensen, Lars Landberg, Jørgen Højstrup, and Helmut P Frank. Wind power meteorology. Risø National Laboratory, Roskilde, Denmark, Technical Document No. Risø-I-1206 (EN), 1997.

Jonathan E Pleim. A combined local and nonlocal closure model for the atmospheric boundary layer. part i: Model description and testing. Journal of Applied Meteorology and Climatology, 46(9):1383–1395, 2007.

Ian A Renfrew and Philip S Anderson. Profiles of katabatic flow in summer and winter over coats land, antarctica. Quarterly Journal of the Royal Meteorological Society, 132(616):779–802, 2006.

Dipl-Kfm Günter Dietmar Roth. Allgemeines literaturverzeichnis. In Technik und Theorie, pages 461–490. Springer, 1989.

Hyeyum Hailey Shin and Song-You Hong. Intercomparison of planetary boundary-layer parametrizations in the WRF model for a single day from cases-99. Boundary-Layer Meteorology, 139(2):261–281, 2011.

C Stallings, RL Huffman, S Khorram, and Z Guo. Linking gleams and gis. Paper-American Society of Agricultural Engineers (USA), 1992.

Roland B Stull. An introduction to boundary layer meteorology, volume 13. Springer Science & Business Media, 1988.

B Tammelin, C Morgan, E Peltola, F Richeft, H Siefert, K Säntti, and P Volund. Wind energy production in cold climate. In EWEC-CONFERENCE-, pages 347–353, 1997.

Alfred H Thiessen. Precipitation averages for large areas. Monthly weather review, 39(7):1082–1089, 1911.

Gregory E Tucker, Stephen T Lancaster, Nicole M Gasparini, Rafael L Bras, and Scott M Rybarczyk. An object-oriented framework for distributed hydrologic and geomorphic modeling using triangulated irregular networks. Computers & Geosciences, 27(8):959–973, 2001.

IGNAZ Vergeiner and EKKEHARD Dreiseitl. Valley winds and slope winds̊Uobservations and elementary thoughts. Meteorology and Atmospheric Physics, 36(1-4):264–286, 1987.

IEA Wind. Expert group study on recommended practices–13. Wind energy projects in cold climates, 2011.

Tetsuji Yamada and George Mellor. A simulation of the Wangara atmospheric boundary layer data. Journal of the Atmospheric sciences, 32(12): 2309–2329, 1975.